Spectroscopic Expression of the External Surface Sites of H-ZSM-5

Laureline Treps, Coralie Demaret, Dorothea Wisser, Bogdan Harbuzaru, Alain Méthivier, Emmanuelle Guillon, Denys Viktorovych Benedis, Axel Gomez, Theodorus de Bruin, Mickaël Rivallan, et al.

Spectroscopic Expression

of the External Surface Sites of H-ZSM-5

Laureline Treps,[1,‡] Coralie Demaret,[1,‡] Dorothea Wisser,[2,†] Bogdan Harbuzaru,[1] Alain Méthivier,[1] Emmanuelle Guillon,[1] Denys Viktorovych Benedis,[1] Axel Gomez,[1,3] Theodorus de Bruin,[4] Mickaël Rivallan,[1] Leonor Catita,[1] Anne Lesage,[2] Céline Chizallet[1,]*

[1] IFP Energies nouvelles – Rond-Point de l'Echangeur de Solaize – BP 3 69360 Solaize, France

[2] Centre de RMN À Très Hauts Champs, Université de Lyon (CNRS/ENS Lyon/UCB Lyon 1), 69100 Villeurbanne, France

[3] Département de Chimie, École Normale Supérieure, PSL University, 75005 Paris, France

[4] IFP Energies Nouvelles, 1 et 4 avenue de Bois-Préau, BP3, 92852 Rueil-Malmaison, France

* celine.chizallet@ifpen.fr

ABSTRACT.

The nature and spectroscopic expression of external surface sites of zeolites, in particular ZSM-5, is a long-debated question. Herein, we use three cutting-edge techniques: Fourier-Transformed Infrared Spectroscopy (FTIR) with Fourier self-deconvolution (FSD), high-magnetic field proton NMR spectroscopy under fast Magic Angle Spinning (MAS) and periodic boundary Density Functional Theory (DFT) calculations to study external surface models and analyze the effect of crystallite size. This provides an unequaled description of the various kinds of hydroxyl groups and of their proximities. The hydrogen-bond donor, acceptor or isolated nature of the hydroxyls results in distinct signals both in FTIR and NMR spectra, but the peak assignment is not the same from one technique to the other when the chemical nature of the hydroxyl changes. Bridging Si-(OH)-Al groups and Al-(H_2O) lead to overlapping signals in one-dimensional ^{1}H MAS NMR, whereas their contributions are strongly different in FTIR spectra. However, quantification and proximity assessment could only be obtained by ^{1}H MAS NMR. With DFT, we confirm previous assignments for silanols and Si-(OH)-Al bridging OH groups. Other signals (between 3750 and 3600 cm^{-1}, and between 1 and 4 ppm) are not only assigned to extra-framework species (which we confirm with dedicated models), but also enclose the signature of sites exposed at the external surface of ZSM-5. In particular, Al-(H_2O) species (~3665 cm^{-1}, 3.8, 2.6 ppm) and Silanol-Al (~3740, 3720, 3665 cm^{-1}, 2.6, 2.2 ppm) contribute to several features depending on their environment. μ_1-Al-OH are also present at the external surface in low amount, with a 3780 cm^{-1} signal in IR, and weak signals in the 0-2 ppm interval in ^{1}H MAS NMR.

KEYWORDS: Zeolite, DFT, surface sites, NMR, infra-red, hydroxyl, silanol

1. INTRODUCTION

Zeolites are microporous aluminosilicates, defined as materials exhibiting pore diameters < 2 nm. They are described as 3D frameworks of SiO_4 tetrahedra. Al^{3+} cations occupy Si^{4+} crystallographic positions, requiring charge compensation cations that give birth to the chemical reactivity of zeolites. This is why these solids are widely employed in refining, petrochemistry, pollution abatement and biomass conversion, among other applications.[1-6] In the case where the compensating cation is a proton (H^+), it gives rise to a hydroxyl group, bridging between a silicon and an aluminum atom (Figure 1-a). These sites are considered as the Brønsted acid sites of the protonic zeolite. ZSM-5 (Zeolite Socony Mobil-5[7]) is one of the most used and studied zeolites, both from fundamental and industrial points of view. Many model studies have been proposed to better understand the structure and reactivity of ZSM-5, based on the consideration of very big zeolite particles (sized several μm) with a well-defined shape that makes the understanding of their inner structure possible.[8-12] However, zeolite particles that are used for industrial applications exhibit much smaller crystal sizes. In particular, zeolite nano-sheets,[13-15] nano-crystals[16-17] (~100 nm) and even embryonic zeolites[18-19], so small that they do not induce any X-Ray diffraction signature, currently attract a lot of attention. The main motivation for the small crystallite size is the expected reduction of diffusion time to reach the acid sites located at the particle center. For such systems with increased surface/volume ratio, the role of the external surface of the crystallites cannot be neglected. For bulky reactants, it is actually considered that catalysis takes exclusively place at the pore mouth,[20-23] with a specific selectivity.[24] The structure of the acid sites located at the external surface remains, however, a matter of debate.[25] Our goal is to unravel the nature of these external surface OH groups, thanks to an approach combining DFT calculations, infra-red and nuclear magnetic resonance experiments.

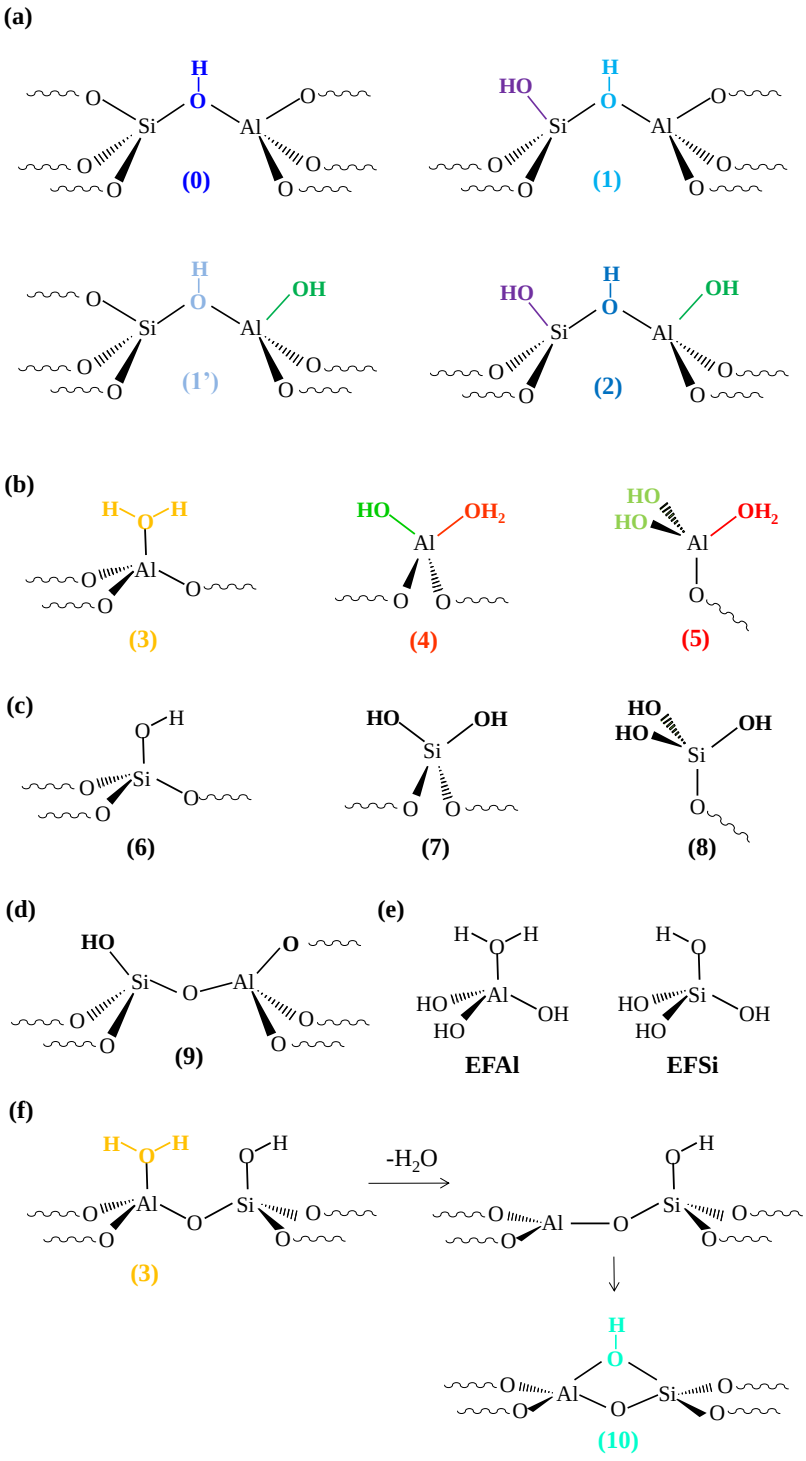

Figure 1. Environment and terminology of the various hydroxyl groups modeled by DFT in this work. (a) bridging Si-(OH)-Al group, known to be present in the bulk and at the external surface, with various possible second neighbors. (b) water molecules adsorbed at surface aluminum, at the external surface,[26-27] with possible Al-OH neighbors. (c) Silanols. (d) Silanol-Al.[28-29] (e) Mononuclear model extra-framework species, hosted in the zeolite porosity. (f) Dehydration of an Al-(H_2O) site giving an Al_{III} close to a silanol, that then forms a 2MR upon Si-(OH)-Al bridge closure.

Infrared (IR) spectroscopy is a relevant and frequently used method to analyze hydroxyl groups, as the stretching frequency of the O-H bond is sensitive to the environment of the hydroxyl, in terms of coordination number of the oxygen, of nature of the cation to which it is bonded, and of the hydrogen-bond network.[30-31] Infrared spectra of ZSM-5 exhibit features that are usually assigned from empirical considerations to several kinds of bridging OH groups (~3610 cm^{-1}), silanols (~3740 cm^{-1}, Figure 1-c), as well as various kinds of poorly defined framework, extra-framework and defect species (~3700-3650 cm^{-1}, Figure 1-e).[31-42] In some cases a broad absorption band is observed between 3400 and 3700 cm^{-1}, linked to silanol nests and adsorbed water.[43-44] Hoffmann et al.[43] proposed a more detailed assignment for the 3740 cm^{-1} region assigned to silanols, on the basis of the intensity and width of the bands. They expect external silanols to vibrate at high frequency: free or terminal silanols are proposed to appear at 3747 cm^{-1}, geminal silanols at 3742 cm^{-1}. Internal silanols are expected at lower frequencies (3730-3700 cm^{-1}), with a possible influence of aluminum atoms (sometimes hypothesized to be tricoordinated) connected to these silanols (then vibrating at 3730 cm^{-1}) via Si-O-Al bridges.[43] The sites were called Silanol-Al[28-29] (Figure 1-d) and were also invoked for amorphous silica-alumina previously.[45] A drawback of IR spectroscopy is the need to know the extinction coefficient for each kind of surface OH group to quantify them. The determination of these coefficients is not straightforward and their values differ a lot from one study to another.[30,46] Issues related to the choice of the baseline before deconvolution also render the integration operator-dependent.

Nuclear Magnetic Resonance (NMR) spectroscopy is a powerful analytical tool for the structural characterization of zeolites. ^{27}Al Magic Angle Spinning (MAS) NMR is widely used to characterize the coordination of aluminum sites in a qualitative and quantitative manner. Tetra-coordinated aluminum atoms Al^{IV} usually resonate between 70 and 40 ppm, while hexa-coordinated aluminum atoms Al^{VI} are found in spectral region ranging from 10 to

-20 ppm.[47] However, due to the second-order quadrupolar broadening, ^{27}Al resonances often overlap, which prevents the observation of clear-cut NMR signatures. The development of ^{27}Al Multi-Quantum (MQ) MAS NMR techniques[48-49] has led to a significant improvement of spectral resolution, allowing one to distinguish between nonequivalent sites in zeolite frameworks. Several studies have reported on the existence of different T sites on ZSM-5 using ^{27}Al MQ-MAS technique.[50-51] Recently, by applying the same technique at very high magnetic field (22.3 T), Holzinger et al.[52] were able to identify 10 nonequivalent framework Al^{IV} sites in ZSM-5 zeolite with different Si/Al ratios (15-140) before and after steam treatment.

^{1}H Magic Angle Spinning Nuclear Magnetic Resonance spectroscopy (^{1}H MAS NMR), although less frequently applied, also provides valuable structural insights on the OH groups.[53-63] Three main regions are usually observed in ^{1}H NMR spectra of dehydrated H-ZSM-5 zeolite:[64-69] bridging OH groups resonances are expected at around 4 ppm, isolated or hydrogen-bond acceptor silanols between 1.3 and 2.2 ppm, whereas Al-OH groups associated with extraframework aluminum (EFAl) are assumed to give rise to an intermediate signal close to 2.6 ppm. Broad signals at 5-6 ppm are usually assigned to adsorbed water molecules. Besides the nature of the acidic OH groups, ^{1}H MAS NMR spectroscopy also gives information about the concentration of hydroxyl groups, which can be derived from the intensities of the resonances. This is an advantage with respect to infrared spectroscopy. Additionally, ^{1}H double-quantum (DQ) NMR spectroscopy can be applied to probe spatial ^{1}H-^{1}H proximities between hydroxyl groups.[70] Thus, this technique was recently used to reveal close proximities between Brønsted and Lewis acid sites in dealuminated H-ZSM-5 zeolites.[71-72]

For both types of spectroscopy, removing physisorbed water is required to minimize the hydrogen-bond network, hence revealing sharper signals that can be more specifically

assigned to the various kinds of OH groups. Despite these efforts, strong uncertainties remain for an accurate assignment of both the IR and NMR signatures corresponding to the non-ideal sites (i.e., different from bulk bridging OH groups), as the structure and environment of these sites is still poorly defined. This is especially true for external surface sites, relevant in zeolites of small crystal size.

First principles calculations have proven helpful for the assignment of infrared and ^{1}H MAS NMR spectra of various hydroxylated inorganic systems,[29,73-84] including H-ZSM-5 bulk sites. [41-42,85-87] The investigation of surface hydroxyls of zeolites is however much scarcer.[25] Recently, some of us have established models for the external surface of the ZSM-5 zeolite thanks to Density Functional Theory (DFT) calculations that comprehensively consider the effect of the surface orientation ((100), (010) and (101)), and that of the location of the {Al, H} pairs[27] on the structure of hydroxyl groups. Several kinds of surface sites have been identified. Bridging Al-OH-Si groups (Figure 1-a) were shown to be present at the pore mouth with similar or higher stability than those in bulk sites. However, at the outermost surface, the following groups prevail: Si-OH, Al-OH groups, and most importantly water adsorbed on aluminum Al-$(H_2O)(OH)_n$ (n=0-2) (Figure 1-b). These groups have however so far escaped unambiguous spectroscopic observations and identification.

The aim of the present work is to unambiguously identify, thanks to a combination of DFT calculations and dedicated IR and NMR experiments, the spectroscopic expression of external surface OH groups in zeolites. Hydroxylated ZSM-5 zeolites free from physisorbed water were considered. FTIR with Fourier self-deconvolution (FSD) and high-magnetic field ^{1}H NMR experiments were conducted on two samples of different crystal sizes (but of similar Si/Al ratio) to unambiguously decipher the signature of the external surface. By taking advantage of surface models established recently by some of us,[27] as well as by developing new models for extraframework species, DFT calculations were performed to predict both the

IR frequencies and ^{1}H NMR chemical shifts of every possible kind of hydroxyls. Previous empirical assignments were largely refined, allowing one to provide a comprehensive and detailed description of the spectroscopic signature of the external surface sites. Double quantum (DQ) NMR experiments were finally interpreted in the light of these new assignments.

2. EXPERIMENTAL METHODS AND COMPUTATIONAL SECTION

2.1. DFT calculations

Periodic DFT calculations were performed with the PBE (Perdew, Burke, and Ernzerhof) exchange-correlation functional[88] as implemented in VASP 5.4.1.[89-90] The projected augmented wave (PAW) method[91] was used to describe the core-electron interactions. Depending on the kind of calculations performed, the plane wave basis set was limited to a kinetic cutoff energy of 400-800 eV. A density dependent dispersion correction, dDsC,[92] was applied. It was chosen due to the good agreement of the MFI cell parameters optimized with PBE-dDsC with respect to experiments (see below), and as the ^{1}H NMR prediction led to fruitful results with this functional in the case of alumina surface models.[76] The convergence criterion for the electronic self-consistent field relaxation was fixed to 10^{-5} eV. All calculations were performed at the Γ-point. Full geometry optimizations were performed using a conjugate-gradient algorithm, with a convergence criterion on forces of 0.02 eV.Å^{-1}.

The bulk cell parameter and initial ionic positions of ZSM-5 (MFI) were obtained from the International Zeolite Association database[93] and then reoptimized in the purely siliceous form with an increased energy cutoff of 800 eV. The final values are (almost orthorhombic α=89.99°, β=90.00°, γ=90.00°): a=20.009 Å, b=19.901 Å and c=13.364 Å, in reasonable agreement with the experimental values[94-95] (orthorhombic: a=20.07 Å, b=19.92 Å

and c=13.42 Å). These values were then kept constant throughout the study. The bulk configuration exhibits 12 inequivalent T sites in the structure. The slab construction is performed following the methodology of our previous works.[26-27] The structure is cleaved along three different orientations ((100), (010), and (101)), which were determined to be the main surfaces observed experimentally for ZSM-5 crystals.[9,96-97] The thickness of the slab was set at two bulk units with a 25 Å vacuum layer. Finally, the surface was saturated with OH groups; hydrogen was added to monocoordinated O atoms and OH moieties saturated Si_{III} atoms. The alumination of the bulk and surface structures was represented by the replacement of one silicon by an aluminum in one of these positions. H^+ was added as a compensation cation on one of the oxygen neighbors of aluminum.

Harmonic frequency calculations were performed with an energy cutoff of 400 eV on optimized structures under the same conditions, with a displacement of ±0.005 Å around the equilibrium atomic positions. For aluminated slabs, the atoms allowed to vibrate were the OH group containing the compensation cation, the Al/Si first neighbor, all O second neighbors, Si third neighbors, and O fourth neighbors.

Chemical shifts were calculated with the linear response approach, using the gauge including projector augmented wave (GIPAW) formalism.[98-99] The step size for the finite difference **k**-space derivative was set to 0.003. First order finite difference stencil was used to calculate the magnetic susceptibility. The average of the isotropic chemical shielding (σ_{TMS}) of each proton of a single tetramethylsilane in vacuum (20 $Å^3$ box) was used as a reference to calculate the isotropic chemical shift δ_{iso} of the various protons at the surface of ZSM-5, from their isotropic chemical shielding (σ_{iso}):

$$\delta_{iso} = \sigma_{TMS} - \sigma_{iso} \qquad \text{Eq. (1)}$$

2.2. Samples and general characterization

The ZSM-5 zeolites were provided by Zeolyst and hereinafter referred as Z-22-Big (meaning: ZSM-5 sample with a Si/Al ratio of 22, see below, and big particles) and Z-25-Small. The zeolites were calcinated before use for 2 hours at 873 K (5 K/min ramp) under air flush. The overall Si/Al ratio of the zeolites was obtained by X Ray Fluorescence (XRF) using an ARL PERFORM'X Sequential X-Ray Fluorescence Spectrometer from ThermoFisher Scientific. The Si/Al ratio of the zeolites near the surface (up to 10 nm) were obtained by X Ray Photoelectron Spectroscopy (XPS) using an ESCA KRATOS Axis Supra Spectrometer. The textural properties of the zeolites were determined by physisorption of nitrogen combined with electron microscopy (Scanning Electron Microscopy: SEM, Nova NanoSEM™, and Transmission Electron Microscopy: TEM, JEOL JEM-2100F, bright field). Microscopy images (SEM and TEM) make it possible to describe the morphology of the crystals and estimate their theoretical external surfaces. A Micromeritics 2020 ASAP gas adsorption analyzer was used for nitrogen sorption measurements. Prior to analysis, the samples were outgassed for 1 hour at 373 K and for 4 hours at 723 K under secondary vacuum (1.10^{-5} mbar). Specific surface areas were determined from the BET equation. The total pore volume is the nitrogen volume adsorbed at $P/P_0 = 0.99$. The t-plot method was used to obtain the microporous volumes of the samples.

2.3. Infrared spectroscopy

The IR investigations were carried out using a Bruker Vertex 70 spectrometer at a spectral resolution of 4 cm^{-1} and accumulating 64 scans. Self-supporting pellets (≈10 mg cm^{-2}) were prepared by pressing sample powders at 0.5 tons and were treated under vacuum ($<10^{-5}$ mbar) in a homemade IR glass cell. A spectrum of the sample was recorded at 298 K after thermal treatment under secondary vacuum ($<10^{-5}$ mbar) every 50 K from 423 up to 673 K (the sample was left for 1h for each temperature step). Fourier self-deconvolution (FSD) of

the IR spectra was performed on Thermo Omnic software in the 4000 – 2500 cm^{-1} spectral range, using a line bandwidth of 10 cm^{-1} (width of the contribution at the half-height) and an enhancement factor of 2 (ratio of the bandwidth before and after FSD treatment).

2.4. Nuclear Magnetic Resonance

Room temperature ^{27}Al MAS NMR single pulse spectra and ^{27}Al Multiple-Quantum Magic-Angle Spinning (MQ-MAS) two-dimensional spectra were recorded on a Bruker Avance III 400 wide bore spectrometer operating at a static field of 9.4 T. The ^{27}Al NMR frequency was 104.22 MHz. All samples were fully hydrated in a saturator for one night prior to measurements and packed in 4-mm zirconia rotors. ^{27}Al MAS NMR single pulse spectra were acquired at a spinning rate of 12 kHz, a pulse length of 1 µs (π/20) and a pre-scan delay of 1 s, which ensured a quantitative analysis. ^{27}Al MQ-MAS spectra were performed using the z-filtered pulse sequence[100] synchronized to the spinning rate (equal to 14 kHz).[101] This sequence consists of two hard-pulses of 4 µs and 1.5 µs at an radiofrequency (rf) field of 190 kHz and a soft selective pulse of 11.5 µs length (at a rf field of 22 kHz). 96 increments were defined in the indirect dimension t_1 with 9216 scans each. A pre-scan delay of 0.25 s was set. Spectral processing including shearing procedure was done using Topspin. The isotropic chemical shifts and the respective quadrupolar constants were obtained by deconvolution of the 2D spectrum using DMfit software,[102] which allowed obtaining the relative amount of each aluminum site. The ^{27}Al chemical shift was referred to a saturated $Al(NO_3)_3$ solution.

Proton one-dimensional (1D) and two-dimensional (2D) double-quantum single-quantum (DQ-SQ) correlation experiments were performed at room temperature on a Bruker Avance III 800 narrow bore spectrometer operating at a magnetic field of 18.8 T (800 MHz ^1H resonance frequency). Prior to signal acquisition, the samples were pretreated under secondary vacuum (<1.10^{-5} mbar) at 573 K for 10 hours and sealed in a glass reactor. The

dehydrated samples were then packed into 2.5 mm zirconia rotors under inert conditions. All ^{1}H spectra were acquired at a spinning rate of 30 kHz. One-dimensional ^{1}H experiments were acquired using a DEPTH[103-105] pulse sequence, consisting of a π/2 pulse of 2.5 μs length followed by two π pulses, by which probe background signals are suppressed. To ensure a quantitative analysis, a pre-scan delay of five times the ^{1}H longitudinal relaxation time (T_1) was applied. Spectral deconvolution was carried out using DMFit.[102] For ^{1}H DQ-SQ NMR experiments, the back-to-back (BABA) recoupling sequence[106] was chosen for excitation and reconversion of the double quantum coherences. The experiments were recorded using 128 increments in the indirect dimension t_1 with 32 scans each. π/2 pulses of 2.5 μs length were used and the inter-scan delay was set to 2 s. The ^{1}H chemical shifts were referenced to the single resonance observed for protons of (external) adamantane at 1.87 ppm.

3. RESULTS and DISCUSSION

3.1. Surface OH groups calculated by DFT

We investigated the properties of bulk sites and of surface sites modeled at different cleavages of ZSM-5 cut in the (100), (010) and (101) orientations (Figure S1 in Supporting information). We chose to investigate the sites of (010) and (101) orientations that are located on the most stable surfaces found under typical conditions of temperature and water pressure (cleavage 2 and cleavage 6 respectively, see ref. [27]). Conversely, all the stable surfaces appearing on the stability diagram in ref. [27] are considered for the (100) orientation (cleavages 1, 6 and 10).

In perfectly crystalline bulk models, only bridging Si-(OH)-Al groups are present. We also found bridging groups Si-(OH)-Al at the surface. These surface Si-(OH)-Al groups are not all structurally equivalent, depending on the neighborhood of the oxygen linked to the Si and Al (first cationic coordination sphere, Figure 1-a). We show in the following that this may lead

to subtle differences in the spectroscopic features of the corresponding Si-(OH)-Al groups. The neighbors may be: framework oxygen atom as in the bulk, hydroxyls linked to the aluminum or linked to the silicon atom of the bridging OH group.

We also found at the external surface water molecules adsorbed on aluminum with or without neighboring hydroxyl groups $Al(H_2O)(OH)_n$ (n=0 to 2, Figure 1-b).[27] Aluminols and silanols appear in structures depicted in Figure 1-a-b. For n=0, the dehydration of $Al(H_2O)$ was shown to generate Al_{III} sites.[27] The latter are close to Si-OH groups. In the case of the surface of mordenite, Bucko et al. proposed that a Si-(OH)-Al bridge can close upon bonding between the Si-OH and the Al_{III}.[74] This generates a two-membered ring (2MR) (Figure 1-f and Figure 2-a), where the aluminum is linked to one of its silicon second neighbor by two oxygen atoms, including one linked to a proton. Such a situation was also shown to take place in the case of the (101) surface of ZSM-5.[107] In the present work, we evaluated this possibility at three locations (see terminology in ref. [27]): the Si59 site of the (100) surface cleavage 1, the Si87 site of the (100) surface cleavage 1 and the Si45 site of the (010) cleavage 2, and found that it corresponds to reaction energies of 3.4 kJ/mol, 0.2 kJ/mol and -4.3 kJ/mol respectively. So, the two kinds of defects (Al_{III} versus 2MR) have very similar probability existence, in agreement with previous findings.[74,107]

Several kinds of environments exist for the many silanols existing at the surface (Figure 1-c). They may be terminal, vicinal or geminal, or three on the same silicon. Those linked to Al atoms via Si-O-Al bridges (Figure 1-d) are called Silanol-Al. They are considered hydrogen-bond donor when the O-H···O non-covalent bond is smaller than 2.5 Å.

Monomeric extra-framework species represented in Figure 1-e were modeled (one monomer per simulation cell): $Al(OH)_3H_2O$ as alumina monomer and $Si(OH)_4$ (orthosilicic acid) as silica monomer. These monomers are studied in interaction with the bulk zeolite, and with its external surface. A bulk and a surface cell (cleavage 1 of orientation (100)),

following the terminology given in ref. [27]) of ZSM-5 with one T5 (IZA terminology) aluminated site is taken and the monomers are inserted into the structure in different ways to explore the different possible interactions. Each monomer may interact in different ways with the zeolite framework. The spectroscopic calculation included each possible case of interaction modeled. EFAl and EFSi can form a covalent bond (chemisorption) with a silicon or an aluminum atom, and this covalent bond can go along with a protonation of the zeolite structure or not. Therefore, the formation of a covalent bond between the zeolite structure and a monomer gathers 16 different possibilities, which are all included in this study. The second possible interaction with the zeolite structure is a physisorption of the monomers, which can also go along with a protonation of the zeolite structure or not. Consequently, there are also 16 different possibilities for the physisorption interaction which are also included in this study.

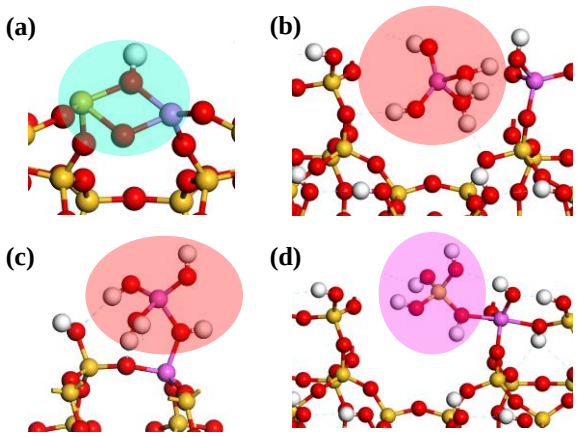

Figure 2. Examples of sites modeled by DFT calculations : (a) 2MR formed upon dehydration of the Si87 site of the (100) surface cleavage 1, (b) EFAl at the (100) surface of ZSM-5, after deprotonation of a close Al-(H_2O) site, (c) EFAl at the (100) surface of ZSM-5, after formation of a O-Al covalent bond with a surface Al_{IV} atom (d) EFSi at the (100) surface of ZSM-5, after formation of a O-Al covalent bond with a surface Al_{IV} atom. Red: oxygen, purple: aluminum, yellow: silicon, white: hydrogen.

3.2. Main characteristics of the two zeolite samples

The physical-chemical properties of the two zeolites samples after calcination are summarized in Table 1. Z-22-Big has a type I isotherm, characteristic of purely microporous

materials. In contrast, the nitrogen physisorption isotherm of Z-25-Small is type IV characteristic of a micro-mesoporous material (Supporting Information S2).

Table 1. Physical-chemical properties of the zeolite powders.

Sample		**Z-22-Big**	**Z-25-Small**
Na (ppm)[a]		209	230
Si/Al global (mol/mol)[b]		21.6 +/- 4.5	24.7 +/- 5.5
Si/Al surface (mol/mol)[c]		18.7 +/- 1.3	22.0 +/- 1.3
Crystal size (nm)[d]		2000 × 1000 × 400	40 × 40 × 40
V_{micro} (cm^3/g)[e]		0.177	0.159
V_{total} (cm^3/g)[e]		0.210	0.360
S_{BET} (m^2/g)[e]		409	408
S_{ext} (m^2/g)[e]		11	47
S_{ext} (m^2/g)[f]		4	88
%Al site[g]	Al^{VI}_1	6	0
	Al^{IV}_1	74	43
	Al^{IV}_2	13	39
	Al^{IV}_3	7	18

[a] determined by AAS (atomic absorption spectrometry)
[b] determined by XRF (X Ray Fluorescence)
[c] determined by XPS (X-ray Photoelectron Spectroscopy)
[d] determined by SEM (Scanning Electron Microscopy)
[e] determined by nitrogen sorption analyses
[f] estimated from the crystal size (SEM)
[g] obtained from ^{27}Al MQ-MAS (see Table S1 for details)

The highest total pore volume for the sample Z-25-Small is due to the presence of intercristalline mesopores generated by the stacking of small crystals as shown by SEM, but also to the presence of some intracristalline mesopores as can be seen on the TEM images (Figure 3-a to c). The Z-22-Big zeolite presents the characteristic coffin shape of the ZSM-5 crystals, with approximate dimensions : 2 × 1 × 0.4 µm (Figure 3-d). Starting from the crystal size obtained from the SEM images and considering that the crystals are very close in size, we can estimate their external surface area.[108] In our case considering the Z-25-Small as cubic crystals (40 × 40 × 40 nm) and the Z-22-Big as parallelepiped crystals (2 × 1 × 0.4

µm), we obtain the corresponding external surface of 88 $m^2.g^{-1}$ for Z-25-Small and 4 $m^2.g^{-1}$ for Z-22-Big showing the same trends as the values obtained from the nitrogen physisorption (47 and respectively 11 $m^2.g^{-1}$), although crystal agglomeration may explain the deviation obtained for Z-25-Small.

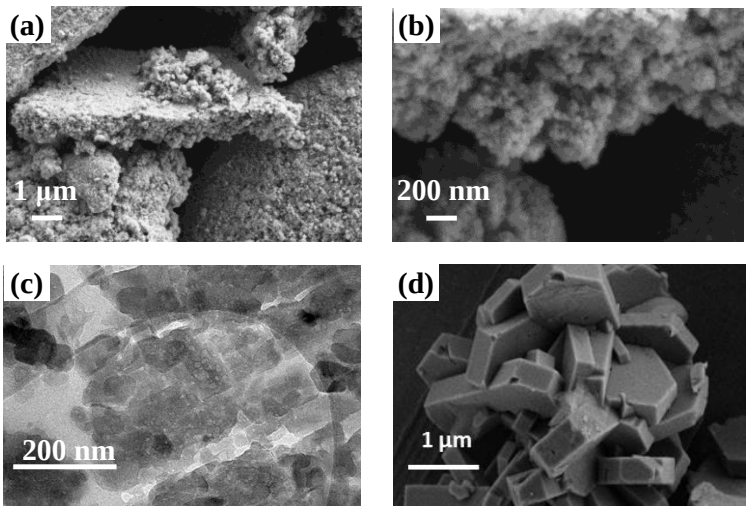

Figure 3. (a), (b) SEM and (c) TEM pictures of the Z-25-Small crystals. (d) SEM image of the Z-22-Big crystals.

By comparing the Si/Al ratio obtained by XRF (global) and XPS (near surface) we can estimate if there is a variation in the crystal composition (center *versus* near surface). The values obtained are present in Table 1. Considering the measurement error we estimate that only the sample Z-22-Big has a small variation in the Si/Al molar ratio, the center of the crystal exhibiting a higher Si/Al ratio than the surface. Notably, considering the very large Si/Al ratio range that ZSM-5 may have (from 8 [109] to infinity[110]), 22 and 25 are actually very close values. ^{27}Al MAS NMR was performed on hydrated samples and shows that most aluminum species are tetrahedral, with negligible amount of octahedral species (Figure S3). For both zeolites, ^{27}Al MQ-MAS spectra (Figure S4 and S5) show three resolved contributions in the region of tetra-coordinated aluminum atoms (Al^{IV}_1, Al^{IV}_2 and Al^{IV}_3) with isotropic chemical shifts (δ_{iso}) between 54 and 57 ppm (see Table S1 for further details). The quadrupolar coupling constants (C_Q) are relatively small (from 1200 kHz to 1300 kHz),

indicating that these sites are in a symmetric environment. The main difference between the two samples concerns the relative intensity of each tetra-coordinated aluminum site (Table 1). The relative proportion of Al^{IV}_1 site is indeed much more important in Z-22-Big than in Z-25-Small. Moreover, ^{27}Al MQ-MAS confirms that only Z-22-Big zeolite exhibits a low intense peak in the region of hexa-coordinated aluminum atoms with a chemical shift of around -1 ppm (Al^{VI}_1). The small C_Q (834 kHz) associated to this aluminum site indicates a weak quadrupolar interaction.

3.3. Infrared feature of surface groups

3.3.1. General features

Infrared spectroscopy has been used in order to determine the evolution of the nature and concentration of the different hydroxyl groups present on the surface of the zeolite crystals upon thermal activation. Spectra of both zeolite samples report the conventional OH features of aluminum containing MFI framework (Figure 4-a and b) whatever the thermal treatment applied (423 – 673 K). Fourier self-deconvolution (FSD) of the interferograms has been done on IR spectra of Z-22-Big and Z-25-Small after thermal activation at 573 K, (Figure 5). FSD mathematical treatment applied on IR spectrum is close to the physical effect observed from NMR characterization of species with slow (solid) and fast (liquid state) relaxation times: the bandwidth of the contribution obtained after Fourier transformation decreases as function of the increase of the free induction decay. FSD treatment artificially enhances the exponential decay factor of the interferogram without the creation of an artificial IR component and consequently allows a “self-deconvolution” of the spectrum from the reduced bandwidth of each individual component.[111] The mathematical FSD treatment evidences the different spectral components present in the hydroxyl region, but it also corrects the baseline of the spectra due to scattering of the IR light on the zeolite crystals.

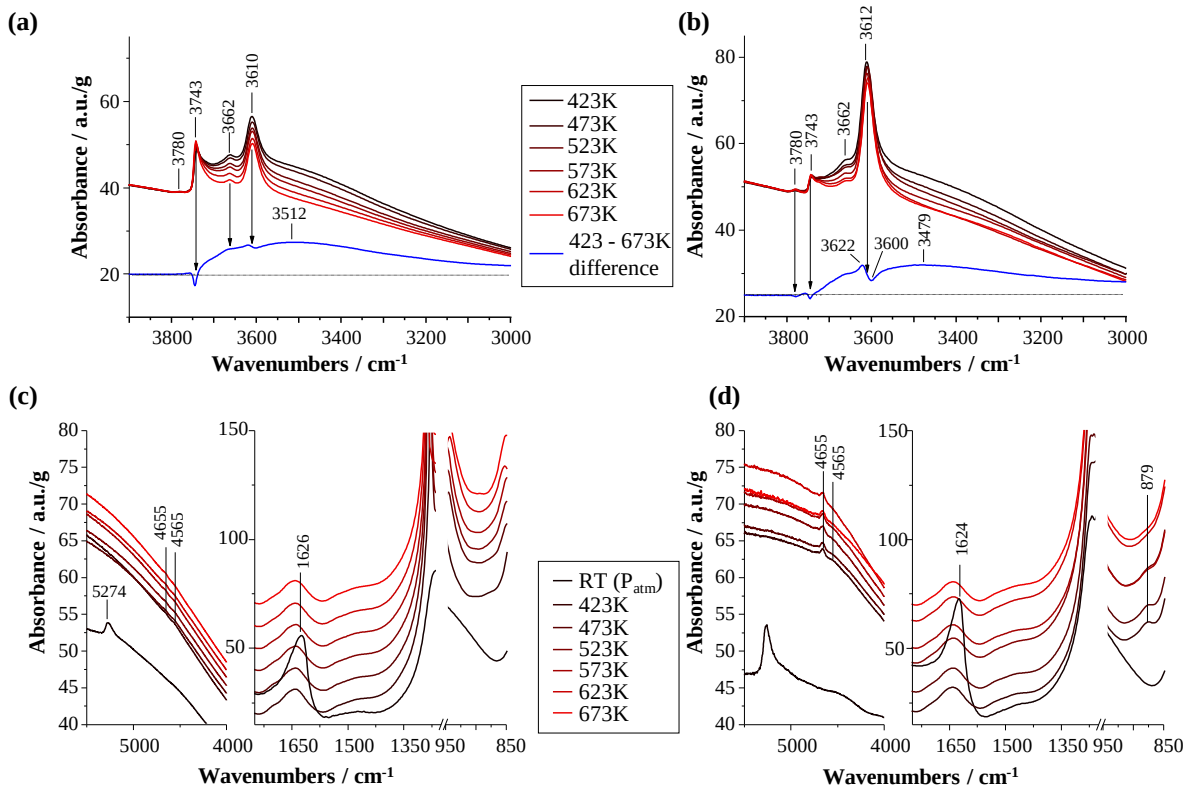

Figure 4. IR spectra of (a)-(c) Z-25-Small, (b)-(d) Z-22-Big, in the O-H stretching region (a)-(b), and in combination band plus bending zone (c)-(d). All spectra are acquired under secondary vacuum.

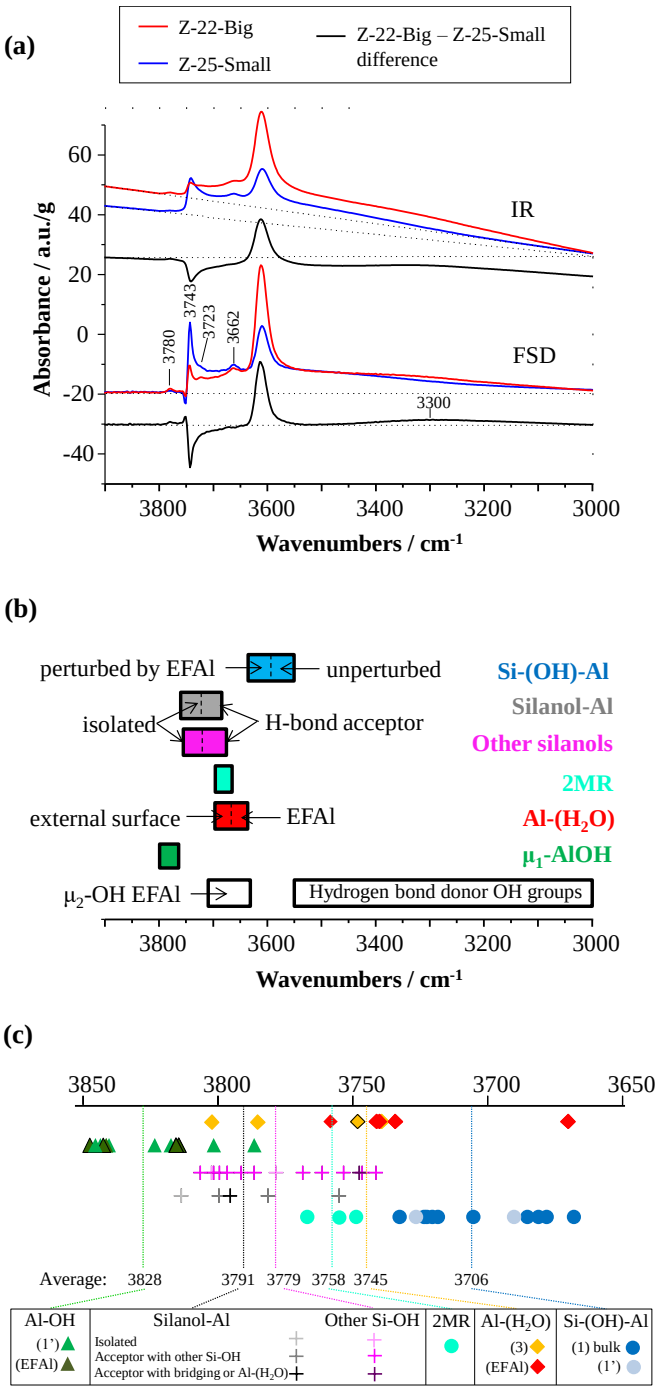

Figure 5. (a) IR spectra before (top) and after Fourier self-deconvolution (bottom) of the two samples activated at 573 K, and their difference. (b) Revised assignment of the IR spectra, from DFT calculations. (c) Harmonic O-H stretching frequencies calculated by DFT for a set of sites. The average for each family is also given. Symbols corresponding to isolated OH groups are circled in black.

Figure 5 also reports the harmonic O-H stretching frequencies calculated by DFT. This spectral zone is well-known to be subjected to contributions from anharmonicity. In the

present work, they are not systematically estimated, assuming that they will not change the order of the individually calculated frequencies. As we expect lower frequencies for hydrogen-bond donor groups,[29,75,78,112-113] we focused our analysis on free and hydrogen-bond acceptor OH groups.

3.3.2. Contributions close to 3610 cm^{-1}

At first, we observe a well resolved contribution located at 3610 cm^{-1} due to the presence of bridging OH groups.[31-42] In DFT, bulk and surface Si-(OH)-Al have a harmonic contribution centered at 3706 cm^{-1} on average (Figure 5-c). This means that the order of magnitude of the anharmonicity shift is close to 100 cm^{-1} for these groups, at the present level of theory. Bulk and surface bridging OH groups do appear in similar spectral zones. The calculated values depend on the level of theory used. In the present work, they are higher than the previous estimations.[42,113] Notably, bridging OH groups belonging to 2MR are not expected to vibrate in a similar spectral zone as other kinds of Si-(OH)-Al groups according to DFT, so that their situation will be described later (section 3.3.4).

The difference in intensity between spectra recorded after activation of Z-22-Big at 423 and 673 K in this spectral zone are only minor. Maxima at 3622 cm^{-1} and minima at 3600 cm^{-1} appear (less significant for Z-25-Small). Because of the presence of an isosbestic point at 3610 cm^{-1}, we could discard the shift of the contribution at 3610 cm^{-1} to lower wavenumbers upon thermal treatment. Moreover, all spectra have been recorded at the same temperature, so that temperature effect on the band width due to vibrational inhomogeneity of the zeolite lattice framework can also be discarded. Thus, the observation of maxima and minima at 3622 and 3600 cm^{-1} instead of 3610 cm^{-1} suggests that below the intense component centered at 3610 cm^{-1}, at least two other contributions at 3600 and 3620 cm^{-1} exist, which are related to a similar surface bridging hydroxyl. This correlates well with our

DFT results: except one group that resonates close to the average value, other calculations lead to two groups of frequencies, separated by about 35 cm^{-1}. From a structural point of view, the bridging hydroxyls vibrating below and above the average value are very similar. The only classification resulting from our DFT calculations is that the signal appearing above average is dominated by bulk bridging OH groups that coexist with EFAls, whereas the one appearing below average corresponds to bridging OH groups that are not perturbed by EFAls.

The two signals evolve upon temperature increase. The 3622 cm^{-1} contribution decreases as the temperature increases. Following DFT calculations, it can likely be assigned to bridging OH groups perturbed by EFAls (although not interacting chemically), that are thus shown to migrate outside the porosity as the temperature increases. The 3600 cm^{-1} signal follows the opposite trend (Figure 4-b), supporting its DFT assignment to bridging OH groups that are not perturbed by EFAls, and which concentration increases as the mobility of EFAls increases.

3.3.3. Contributions between 3750 and 3720 cm^{-1}

At higher wavenumbers, in the 3750 – 3720 cm^{-1} range, IR spectra exhibit a contribution centered at 3743 cm^{-1} usually assigned to silanols. DFT results indicate a distribution of harmonic stretching frequencies of silanols (of all kinds) in the 3815-3740 cm^{-1} interval. This latter interval is too large (75 cm^{-1}) to allow the assignment of the 3720 and 3743 cm^{-1} signals to the whole family of silanols considered in the computational study.

Isolated Si-OH groups resonate at higher frequencies than hydrogen-bond acceptor silanols in average, according to our DFT calculations (Table 2). Isolated Silanol-Al also appear at slightly higher frequency than other kinds of isolated silanols. Notably, we only have one example of isolated Silanol-Al in this study, all others are hydrogen-bond acceptors. This difference between Silanol-Al and other kinds of silanols disappears when these groups

are hydrogen-bond acceptors with neighboring silanols. When the hydrogen-bond donor is a Si-(OH)-Al or a Al-(H_2O) species, silanols are calculated to be strongly red-shifted (3749 cm^{-1}), in agreement with results reported on a DFT model of Amorphous Silica-Alumina.[29]

Thus, it is reasonable to assign the 3720 cm^{-1} contribution mainly to silanols and Silanol-Al that are hydrogen-bond acceptors from other silanols, whereas the 3743 cm^{-1} contribution is expected to correspond to isolated silanols, with a statistical majority of Si-OH different from Silanol-Al, the latter appearing with much lower intensity in this Si/Al range. Notably, the 3720 cm^{-1} resonance was previously assigned to internal silanols (in contrast to external silanols at 3743 cm^{-1}), which is also likely, as internal silanols are expected to be more subjected to hydrogen bonds.[43] However, our work shows that this is not a sufficient assignment. Note also that Zecchina et al. anticipated that hydrogen-bond acceptors appear close to 3730 cm^{-1} on silicalite-1.[37] From our calculations, Silanol-Al that are hydrogen-bond acceptors from an Al-(H_2O) are expected to appear at lower frequency (see section 3.3.4).

The difference between the spectra recorded after activation of the two samples at 423 and 673 K report a negative contribution at 3743 cm^{-1}, revealing an increase of Si-OH concentration upon temperature increase (Figure 4-a-b) that will be further discussed in section 3.3.8.

Table 2. Average vibrational frequency value and proton chemical shift for various kinds of silanols and Silanol-Al groups at the external surface as calculated by DFT.

Group	**Data**	**Isolated**	**H-bond acceptor from another silanol**	**H-bond acceptor from Si-(OH)-Al or Al-(H_2O)**
Silanol-Al	ν_{OH} (cm^{-1})	3815	3780	3797
	δ (ppm)	1.63	2.29	3.03
Other kinds of Si-OH	ν_{OH} (cm^{-1})	3792	3779	3749
	δ (ppm)	1.96	2.46	2.80

3.3.4. Contributions in the 3700 – 3660 cm^{-1} range

In the interval 3690 – 3660 cm^{-1}, between the Si-OH and Si-(OH)-Al stretching OH modes, fall the contributions that are usually assigned to AlOH groups due to the presence of extraframework Al debris and/or Al partially attached to the framework.[114-116] Our DFT analysis refines and partially contradicts this assignment. Indeed, considering both Al-OH from the external surface and from monomeric EFAl (all μ_1-$Al_{IV}OH$), the vibration frequency is calculated to be higher than that of Si-OH. This is expected to correspond to the contribution discussed in section 3.3.5. We cannot exclude the presence of μ_2 aluminols on polymeric EFAls (not simulated here) that could give rise to signals in the 3690 – 3660 cm^{-1} interval, similar to what was found on γ-Al_2O_3 surface models.[79,117] Between silanols and bridging OH groups, DFT predicts that we have, by decreasing frequency order:

- Bridging OH groups belonging to 2MR cycles (Figure 2-a)
- Silanols that are hydrogen-bond acceptors towards Al-(H_2O) in particular (Table 2).
- Al-(H_2O) species at the external surface, and belonging to EFAls at even lower frequency.

Thus, this spectral zone is the signature of the external surface combined with that of EFAls.

3.3.5. Signal at 3780 cm^{-1}

A weak contribution is observed at 3780 cm^{-1} especially evidenced for Z-22-Big after high temperature treatment. It was assigned in the past to OH species of very low acidity and is generally enhanced with severe steaming conditions of HZSM-5 (and HBEA) zeolite at the expense of the acidic bridging OH sites.[118-119]. From probe molecules (acid and base) interaction and looking at different spectral regions (OH and T-O-T modes), Lavalley et al.

proposed to assign this vibration to a basic hydroxyl group on a tricoordinated Al atom partially attached to the framework.[120]

Our DFT investigations suggest that this signal is due to Al-OH groups (μ_1-OH type) at the external surface and at EFAls. Here again, in average, isolated Al-OH appear at slightly higher frequency than hydrogen-bond acceptors. For the latter, the frequency domain is expected to overlap with that of isolated silanols: it is thus likely that the 3780 cm^{-1} band is mainly due to isolated μ_1 Al-OH. This could explain why this band is observed mainly for the Z-22-Big sample, although it exhibits the lower external surface area. It may be due to a weaker hydrogen-bond network due to flatter surfaces with respect to Z-25-Small.

3.3.6. Broad contribution between 3700 and 2800 cm^{-1}

For both samples a very broad signal from 3700 to 2800 cm^{-1} centered close to 3490 +/-15 cm^{-1} is evidenced in the difference spectra. It is due to hydrogen-bond donor OH groups, and possibly to the removal of neutral adsorbed water species. This will be confirmed in the next section by the disappearance of the contribution of υ(OH…O)c mode.

3.3.7. Combination modes and bending zone

At lower wavenumbers (Figure 4-(c)-(d)), a weak contribution located at 880 cm^{-1} is evidenced after evacuation at 423 K for Z-22-Big due to the presence of residual H_2O neutral species.[121] This band does not occur on Z-25-Small, and may imply a stronger confinement of H_2O molecules and hence of the bridging OH groups on Z-22-Big in agreement with the larger size of the crystals. Spectra of both samples at atmospheric pressure and temperature do not report this specific contribution. In the latter condition, zeolite micropores are full of water molecules (see intense $\delta(H_2O)$ and $\upsilon(H_2O) + \delta(H_2O)$ combination modes at ca. 1630 and 5274 cm^{-1} respectively), which lead to proton transfer with formation of $H^+(H_2O)_n$

species. The intensity of the band at 5274 cm^{-1} is about 4 times higher on Z-22-Big than on Z-25-Small in agreement with the larger microporous volume.

The occurrence of the contribution at 880 cm^{-1} due to γ(OH…O) mode is generally accompanied with υ(OH…O) mode at ca. 3696 cm^{-1}.[121] We may note however that the contribution at 3696 cm^{-1} is not very sharp for Z-22-Big after activation at 423 K in agreement with the low intensity of the band found at 880 cm^{-1}. Weak contributions at 4655 and 4565 cm^{-1} are also observed for both zeolites due to (υ + δ) mode combination of Si-(OH)-Al and Si-OH groups respectively. The component at 4655 cm^{-1} is more intense for Z-22-Big in agreement with the higher microporous volume and crystallinity, in line with the higher intensity of the 3612 cm^{-1} band on this sample with respect to Z-25-Small.

3.3.8. Quantitative analysis: impact of crystal size and of temperature

Considering the FSD spectra after activation at 573 K (Figure 5), quantitative comparison of both samples is easier due to the baseline correction. The main differences between the two samples concern the concentrations of Si-OH/Silanol-Al and Si-(OH)-Al species at 3743 and 3610 cm^{-1}. Concentrations (determined from the net intensity measured on the FSD spectra), of Si-OH/Silanol-Al is 3 times higher on Z-25-Small, while concentration of acidic bridging sites is 2 times higher on Z-22-Big. This is in full agreement with the smaller size of Z-25-Small, inducing a higher external surface over crystallite volume ratio, even if the ratio of external surface between Z-22-Big and Z-25-Small is higher than 3 (Table 1), but the latter data suffers from large uncertainties.

From the difference spectra (Z-22-Big – Z-25-Small, FSD) it is seen that the intensity of the contribution located at 3663 cm^{-1} is almost the same for both samples. This was not expressed from the difference of conventional IR spectra, due to signal overlapping of the contribution with higher bandwidth.

After the FSD treatment, the Z-25-Small sample exhibits a more intense shoulder at 3720 cm^{-1} than Z-22-Big. This band characterizes mainly external silanols and Silanol-Al that are hydrogen-bond acceptors from other silanols (section 3.3.3). Thus, Z-25-Small provides more abundant environment promoting hydrogen bonds, in agreement with the defects seen from TEM (Figure 3-c) and less flat surfaces with respect to Z-22-Big.

On the difference FSD spectrum, two contributions are evidenced at 3780 and 3300 cm^{-1} due to a higher concentration of these species on Z-22-Big. The former could be interpreted by the fact that isolated μ_1-Al-OH are more numerous on the flatter surfaces of Z-22-Big. While the latter could be due to the presence of residual H_2O neutral species, in agreement with the remaining contribution located at 880 cm^{-1} at 573 K for Z-22-Big (Figure 4-d).

Peak intensities of the different resonances observed in the FSD-IR spectra have been followed as function of an increase of the activation temperature, 423 – 673 K (Figure 6). The spectra are reported in Figure S7. The evolution of the band at 880 cm^{-1} has been obtained from the IR spectra reported in Figure 4. The concentration of bridging OH groups (3610 cm^{-1}) appears to be preserved upon the temperature increase up to 673 K, in line with the literature,[32] also a redistribution between the 3622 and 3600 cm^{-1} resonances was mentioned in section 3.3.1 and explained by the thermally activated migration of EFAls from the structure. An enhancement of the band located at 3745 cm^{-1} due to isolated external silanols concentration is observed as function of the temperature increase for the two samples. From DFT calculations, this increase can be assigned to the water desorption from Al-(H_2O) sites,[27] that affects the hydrogen-bond network and converts hydrogen-bond donor and acceptor silanols into isolated silanols. For small crystals, Z-25-Small, we also observe a small depletion of hydrogen-bond acceptor silanols (3722 cm^{-1}), and a more significant depletion of the 3450 cm^{-1} band corresponding to hydrogen-bond donor OH groups. The fact that the

decrease of the band at 3722 cm^{-1} is not observed on the Z-22-Big sample could be explained by the lower intensity of these signals (by a factor of more than two), making these less detectable.

The intensity of the contribution at 3663 cm^{-1} decreases as a function of temperature for both samples. From DFT (section 3.3.4), it can be assigned to Al-(H_2O) species, Silanol-Al that are hydrogen-bond acceptors towards Al-(H_2O), 2MR bridging hydroxyls, and possibly μ_2-OH from EFAls. The desorption of water from Al-(H_2O) is expected to induce the depletion of the two former. However, at the same time, the appearance of 2MR sites on some of the Al atoms left dehydrated is expected. The fact that two sites are lost for a third being gained is consistent with the decrease of the intensity of this band as the temperature increases. Notably, the intensity of the 3660 cm^{-1} band is quite similar for both samples (only slightly higher for Z-25-Small), although it is expected to be due at least in part to external surface species. This could be due to the lower surface Si/Al ratio of Z-22-Big, as shown by XPS (Table 1), at the origin of more numerous surface Al on big particles, counterbalancing (for this specific kind of sites) the effect of the lower external surface area.

For Z-22-Big, even if the concentration is low, IR spectra obtained show that the contribution at 3780 cm^{-1} progressively increases as a function of the temperature. According to our DFT assignment, this reveals an increase of isolated μ_1-Al-OH (section 3.3.5) concentration upon temperature increase, again consistently with the depletion of the hydrogen-bond network. This band is hardly detected for the Z-25-Small sample. As argued in section 3.3.5, this may be explained by a denser hydrogen-bond network on this sample.

Thus, our experimental observations and DFT assignments appear to be consistent and enable to explain the main spectral evolutions as a function of particle size and activation temperature. The lack of knowledge of extinction coefficients for the huge variety of groups,

and the overlap between spectral zones characteristic of external surface sites invoked in our assignment, however, motivates the comparison of FTIR with ^{1}H MAS NMR.

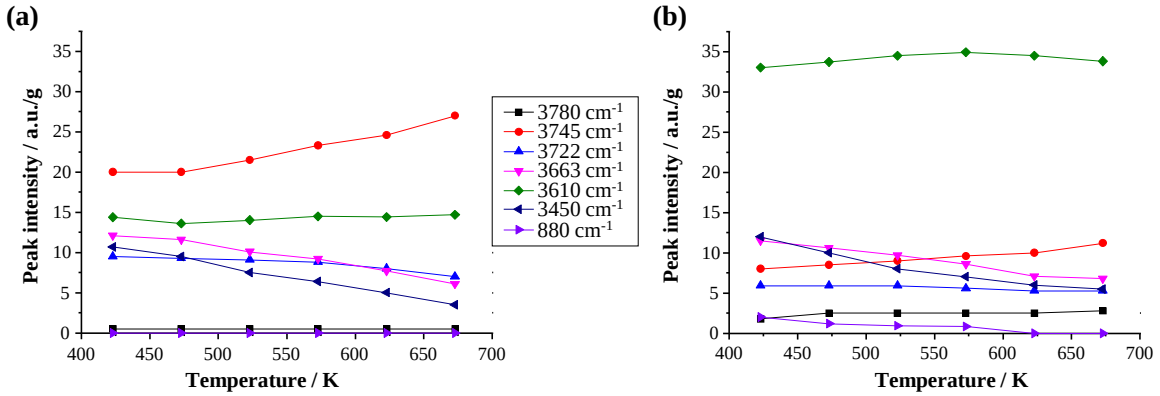

Figure 6. Evolution of the intensity of the different contribution observed in the hydroxyl region of FSD spectra for a) Z-25-Small and b) Z-22-Big as function of the activation temperature.

3.4. ^{1}H NMR feature of surface groups

3.4.1. General feature

Figure 7 shows the 1D ^{1}H NMR spectra of Z-22-Big and Z-25-Small after activation at 573 K, together with the chemical shifts calculated by DFT. Being recorded at a high magnetic field of 18.8 T (800 MHz ^{1}H resonance frequency) and at a MAS frequency of 30 kHz, the spectra are well resolved with respect to usual observations. Similarly, to infrared, calculated chemical shifts are reported for protons which are not hydrogen-bond donors. The latter exhibit very high shifts that are correlated with the hydrogen-bond length (Figure S8), in line with previous observations for other hydroxylated oxides.[76-77,81] However, the chemical shift of protons belonging to hydrogen-bond acceptor hydroxyls are taken into account, as well as that of isolated OH groups. As for the DFT IR results, the calculated chemical shifts are separated in several families: average data for each family are given in Tables 2 and 3. Additional data for silanols are gathered in Supporting Information S4 (Figure S9 and Table S2).

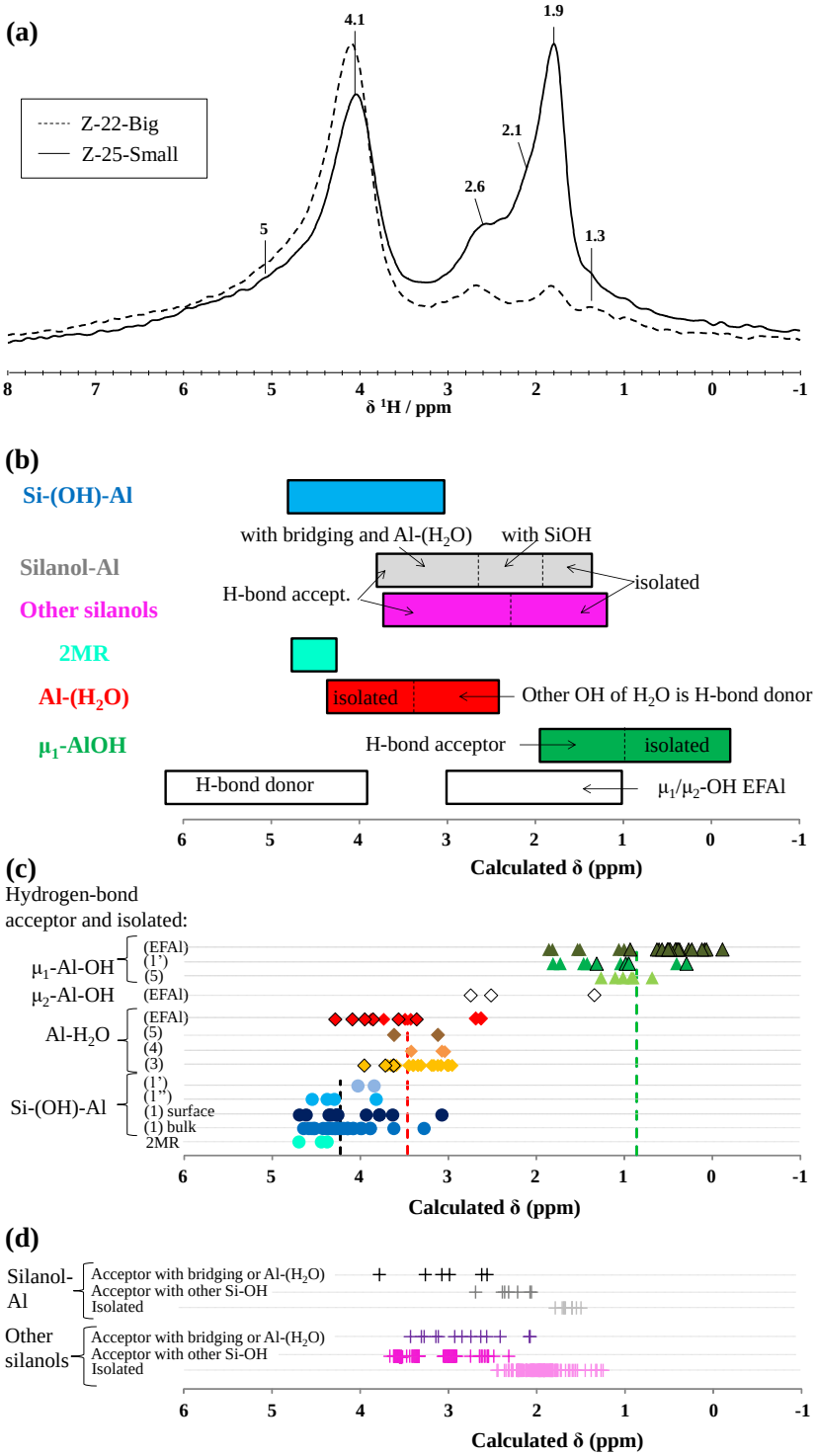

Figure 7. (a) ^{1}H MAS NMR spectra normalized to the mass of the sample of Z-22-Big and Z-25-Small after activation at 573 K. (b) Simplified assignment proposed in the present work on the basis of DFT calculations. ^{1}H NMR DFT calculated chemical shifts of: (c) Al-OH, Al-H_2O, Bridging Si-(OH)-Al, and 2MR sites, (d) Silanol-Al and silanols. For (c), symbols corresponding to isolated Al-OH and Al-(H_2O) are circled in black, and the numbers correspond to the terminology reported in Figure 1. Hydrogen-bond donor OH groups are fully excluded from the diagrams.

The deconvolution of the 1D spectra is shown in Figure S10. Four signals are observed at around to 4.1, 2.6, 1.9 (2.1 and 1.8 ppm for Z-25-Small) and 1.3 ppm, plus a broad contribution centered around 5.1 ppm. The following parts are devoted to the detailed assignment of each of these resonances from the DFT calculations.

Table 3. ^{1}H NMR DFT calculated chemical shifts by family and sub-families, of isolated and hydrogen-bond acceptor hydroxyls. The terminology corresponds to Figure 1. When necessary for the definition of the hydrogen-bond network, a refined structure is presented, the ^{1}H under consideration being depicted with colors. Data corresponding to silanols and silanol-Al are given in Table 2.

Type of site	**Total average (ppm)**	**Sub-family and average ^{1}H chemical shift per category (ppm)**					
Si-(OH)-Al	4.20	(1'): 3.98	(1''): 4.30	(1)- surface: 4.12		(1)- bulk: 4.25	2MR: 4.55
Al-(H_2O)	3.46	EFAl 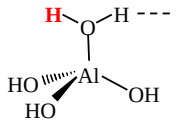 : 3.34	EFAl-isolated: 3.88	(4) 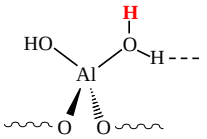 : 3.07	(3) 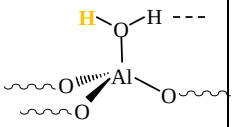 : 3.31	(3)-isolated: 3.76	(5) 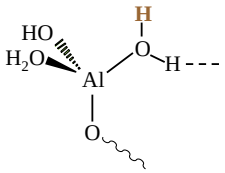 : 3.37
Al-OH	0.86	EFAl 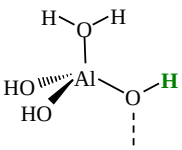 : 1.36	EFAl-isolated: 0.43	(1') 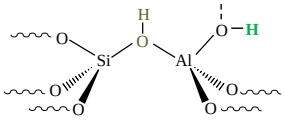 : 1.24		(1')-isolated: 0.93	(5) 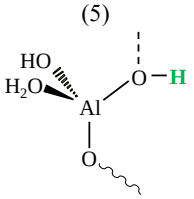 : 1.02

3.4.2. Resonance at around 4.1 ppm

Signals ranging from 3.8 to 4.3 ppm are usually assigned to bridging Si-(OH)-Al groups, which our DFT calculations confirm. Indeed, for bulk bridging OH groups, the calculated ^{1}H chemical shift has an average value of 4.25 ppm. Bridging OH groups at the external surface of the zeolite exhibit a chemical shift average of 4.20 ppm. When second neighbors of the surface bridging OH groups are framework oxygen atoms, as is the case in the bulk, their average chemical shift is found at 4.12 ppm (slightly shielded compared to

bulk bridging OH group). Hydroxyls groups can replace structural oxygen of ZSM-5 and be bound to the aluminum of the bridging OH group, with an average chemical shift of 3.98 ppm, or to the silicon atom, with an average chemical shift of 4.30 ppm. All these values are rather close, and the various bridging groups cannot be distinguished from the 1D ^{1}H spectrum that display a single, broad resonance at 4.1 ppm (Figure 7 and S10).

Notably, bridging OH groups from 2MR sites are expected to appear at 4.55 ppm, thus in the upper chemical shift part of the bridging OH group family. This is in contrast to what is observed in FTIR spectra, where the 2MR signal is clearly differentiated from that of other bridging OH groups, and appears between the frequency of silanols and bridging groups. The trend in NMR is opposite, as 2MR sites are less shielded than other bridging and all silanols (see next sections).

However, DFT results suggest that Si-(OH)-Al groups are not the single species that resonate in the chemical shift range around 4 ppm: water molecules belonging to $Al(OH)_n(H_2O)$ species, either from EFAls or exposed at the zeolite outermost surface, also contribute (Figure 7-b and c). Those exhibiting the chemical shift closer to 4 ppm are isolated water molecules (no hydrogen-bond with the neighborhood), with an average chemical shift of 3.76 ppm for n=0 at the external surface, and of 3.88 ppm in EFAls. Thus, contrary to previous thoughts, the resonance at around 4 ppm does not exclusively correspond to bridging OH groups, but also likely holds part of the signals from Al-(H_2O) species on EFAls and at the external surface.

3.4.3. Resonance at around 2.6 ppm

Resonances centered at around 2.6 ppm are usually assigned to different types of AlOH groups associated with extra-framework species.[56,65-66] The DFT-calculated chemical shifts close to this value belong to (i) water molecules belonging to $Al(OH)_n(H_2O)$ species,

either from EFAl, or exposed at the zeolite outermost surface, when one of the protons is hydrogen-bond donor, and (ii) hydrogen-bond acceptor silanols, either Silanol-Al or all other types, (iii) μ_2-Al-OH, obtained when EFAl monomers bind covalently to surface Al atoms located at the zeolite outermost surface.

Regarding the $Al(OH)_n(H_2O)$ species at the external surface, average chemical shifts of 3.31 ppm (n=0), 3.07 ppm (n=1), and 3.37 ppm (n=2) are calculated for the non-hydrogen-bonded proton of the water molecule, the second being a hydrogen-bond donor (Table 3). Thus, in these cases, the NMR signal shifts by -0.4 to -0.5 ppm with respect to isolated Al-(H_2O) water molecules. The signals of H_2O adsorbed on alumina monomers (EFAl) were also modeled in similar configurations. The average chemical shifts are very similar to the surface $Al(OH)_n(H_2O)$ surface species, with an average value of 3.34 ppm. We note however that a significant fraction of the simulated sites gives rise to signals below 3 ppm (Figure 7).

From Tables 2 and S1, it appears that the chemical shifts of the surface Si-OH groups are not differentiated by the number of neighboring silanols but rather by their isolated *versus* hydrogen-bond acceptor nature. For the latter, the Silanol-Al nature does not impact much. An average chemical shift of 2.48 ppm is calculated, close to the experimental value of 2.6 ppm discussed here. Within the hydrogen-bond acceptor Silanol-Al family, a clear ranking is observed as a function of the nature of the hydrogen-bond donor group. When this donor is a Si-(OH)-Al or Al-(H_2O), the Silanol-Al is characterized by a higher chemical shift (3.03 ppm) than when the donor is another silanol type. The latter resonates at a calculated value of 2.29 ppm, which likely corresponds to the 2.2 ppm signal discussed in section 3.4.4. Isolated silanols (of Silanol-Al nature or other) appear at lower chemical shift, and do not contribute to the presently discussed spectral zone, but to the one discussed below in section 3.4.4.

While simulating the interaction of mononuclear EFAl with the external surface, in some configurations, covalent Al-O bonds were formed that resulted in the formation of μ_2-

Al-OH (in other terms, Al-(OH)-Al), as illustrated in Figure 2-c. Our DFT calculations show that they should appear between 1 and 3 ppm. Notably, on alumina surface and edge models, the same 1-3 ppm spectral zone was assigned to μ_1 and μ_2 OH groups, all linked to aluminum atoms only.[76] Should polynuclear EFAl species be present, they may also participate to the signal close to 2.7 ppm, and possibly also to lower chemical shift signals (see section 3.4.4).

Thus, our DFT investigation drastically expands and refines the empirical assignment of the resonances in this spectral region, usually considered arising only from EFAl Al-OH. Here, we show that Al-(H_2O) groups from EFAls, from external surface sites and from hydrogen-bond acceptor silanols contribute to the signal, as well as μ_1-OH and μ_2-OH groups from EFAls. This very detailed assignment is far less trivial than what is usually considered.

3.4.4. Resonances below 2.5 ppm

Several resonances within the 1.3 and 2.1 ppm range are observed experimentally (Figure 7-a): peaks between 1.8 and 2.1 ppm are usually considered to arise from non-bridging SiOH groups, while minor peaks below 1.5 ppm are attributed to Al-OH species.[122] According to our DFT calculations and by decreasing values of average chemical shifts (Tables 2 and 3), the species that likely contribute to these resonances are (Figure 7-b): (i) some hydrogen-bond acceptor Silanol-Al (when the donor is another silanol, calculated at 2.3 ppm), (ii) isolated silanols and Silanol-Al (at 1.96-1.63 ppm), (iii) hydrogen-bond acceptor μ_1/ μ_2-Al-OH from EFAls (at 1.02-1.36 ppm). (i) and (ii) are likely assigned to the experimentally-observed 2.2 ppm resonance, whereas (iii) better fits with the 1.3 ppm signal.

Indeed, the free silanol groups exhibit a chemical shift average of 1.95 ppm. The chemical shift of isolated OH groups of EFSi adsorbed on the surface, $Si(OH)_4$, are similar with an average value of 1.92 ppm for free hydroxyl groups. Isolated Si-OH appear at higher chemical shifts with respect to Silanol-Al (1.96 *versus* 1.63 ppm). A clear ranking thus

appears between Si-OH and Silanol-Al when these groups are isolated, which disappears (all features being mixed) when these groups are hydrogen-bond acceptors (section 3.4.3). This is very similar to observations made from infrared spectroscopy (section 3.3.3.).

Moreover, a difference is found between the signal of free *versus* hydrogen-bond acceptor μ_1-Al-OH groups. At the external surface, hydrogen-bond acceptor OH from $Al(OH)_2H_2O$ species have a calculated average chemical shift of 1.02 ppm. A signal at 1.24 ppm is found for hydroxyl groups neighboring a bridging group, HO-Al-(OH)-Si. For similar free Al-OH the signal is shifted to an average value of 0.93 ppm. The calculated chemical shift of hydroxyl groups of EFAls exhibits similar trends, with average chemical shift of 1.36 and 0.43 ppm for hydrogen-bond donor and free Al-OH respectively. One isolated μ_2-Al-OH from an EFAl connected to a surface Al atom appears at 1.34 ppm.

Notably, we do not experimentally observe intense resonances lower than 1 ppm, assigned to isolated μ_1-Al-OH groups (from the external surface, from monomeric EFAls, but also from alumina edges[76]), which suggests that such configurations are not abundant in the investigated samples.

3.4.5. Broad signal at higher chemical shifts

The broad signal observed at a chemical shift higher than 5 ppm are usually assigned to strongly adsorbed residual water molecules.[60,65,67] According to our calculations, they may also correspond to the wide family of hydrogen-bond donor groups.

3.4.6. Decomposition of the spectra, analysis of crystal size effects

The absolute and relative fraction of each resonance was extracted from spectral deconvolution (Figures S10 and S11). With increasing crystal size, the intensity of the 1.9 ppm signal decreases from 31% of the total ^{1}H signal to 6%, which is coherent with a higher

external surface area developed by Z-25-Small, as this signal is expected to be mainly due to external silanols. On the contrary, a higher fraction is observed for the signal at around 4 ppm in Z-22-Big (43% versus 25% for Z-25-Small). The ratio of the absolute number of these protons in each zeolite indicates that there are about twice more abundant in Z-22-Big (5467 a.u./$g_{zeolite}$) than in Z-25-Small (2604 a.u./$g_{zeolite}$), in agreement with IR results. This suggests that many aluminum atoms in Z-25-Small, possibly located at the outermost surface, do not form Si-(OH)-Al sites (important contributors to the 4 ppm signal), but rather AlOH groups, Al(H_2O) species or Silanol-Al, as shown by the predominance of the 1-3 ppm signals for this sample.

3.4.7. Two-dimensional proton-proton through-space correlations

Two-dimensional (2D) ^{1}H double-quantum (DQ) NMR spectroscopy was applied to probe spatial proximities between hydroxyl groups (Figure 8). The double-quantum single-quantum experiment yields 2D maps with correlations between pairs of dipolar-coupled (i.e., spatially close) protons. The DQ frequency in the indirect ω_1 dimension corresponds to the sum of the two single-quantum (SQ) frequencies of the two coupled protons and correlates in the ω_2 dimension with the two individual proton resonances. Protons of similar chemical shift yield autocorrelation peaks along the $\omega_1 = 2\omega_2$ diagonal line, while protons with distinct chemical shifts give rise to two off-diagonal peaks.[70] In the following, we analyze the correlation peaks observed experimentally in the 2D DQ-SQ spectra of Z-25-Small and Z-22-Big on the basis of the assignments proposed above.

Figure 8-a shows the DQ-SQ correlation spectrum of Z-25-Small. Three autocorrelation peaks along the diagonal are observed. A first one appears at (ω_1, ω_2) = (3.6 ppm, 1.8 ppm). We previously assigned the signal around 1.8 ppm to isolated silanols and isolated Silanol-Al. The autocorrelation thus reflects spatial proximities between these groups, i.e. between

silanols and Silanol-Al, between Silanol-Al or between silanols. For these latter, this observation is notably in agreement with our calculations on the (101) surface model where isolated silanols are separated by less than 4 Å from each other. Such a configuration, justifying the existence of the autocorrelation peak, is depicted in Figure 9-a.

Another autocorrelation peak appears at (ω_1, ω_2) = (5.2 ppm, 2.6 ppm). The 2.6 ppm resonance was ascribed to Al-(H_2O) with one hydrogen-bonded proton (at the outermost surface or from EFAl), to hydrogen-bond acceptor silanols and Silanol-Al (at the outermost surface or from EFSi) and to μ_2-Al-OH (EFAl). The EFAl groups would justify per se the existence of the autocorrelation peak. At the external zeolite surface, the proximity of free protons from two different Al-(H_2O) groups is very unlikely, due to the rather high Si/Al ratio. In contrast, spatial proximities between Al-(H_2O) groups and a H-bond acceptor Silanol-Al as depicted in Figure 9-b are highly probable and could also contribute to the autocorrelation peak. Finally, a close contact between EFAl and silanols and/or surface Al-(H_2O) could be considered to explain the autocorrelation peak, which some of the DFT models confirm.

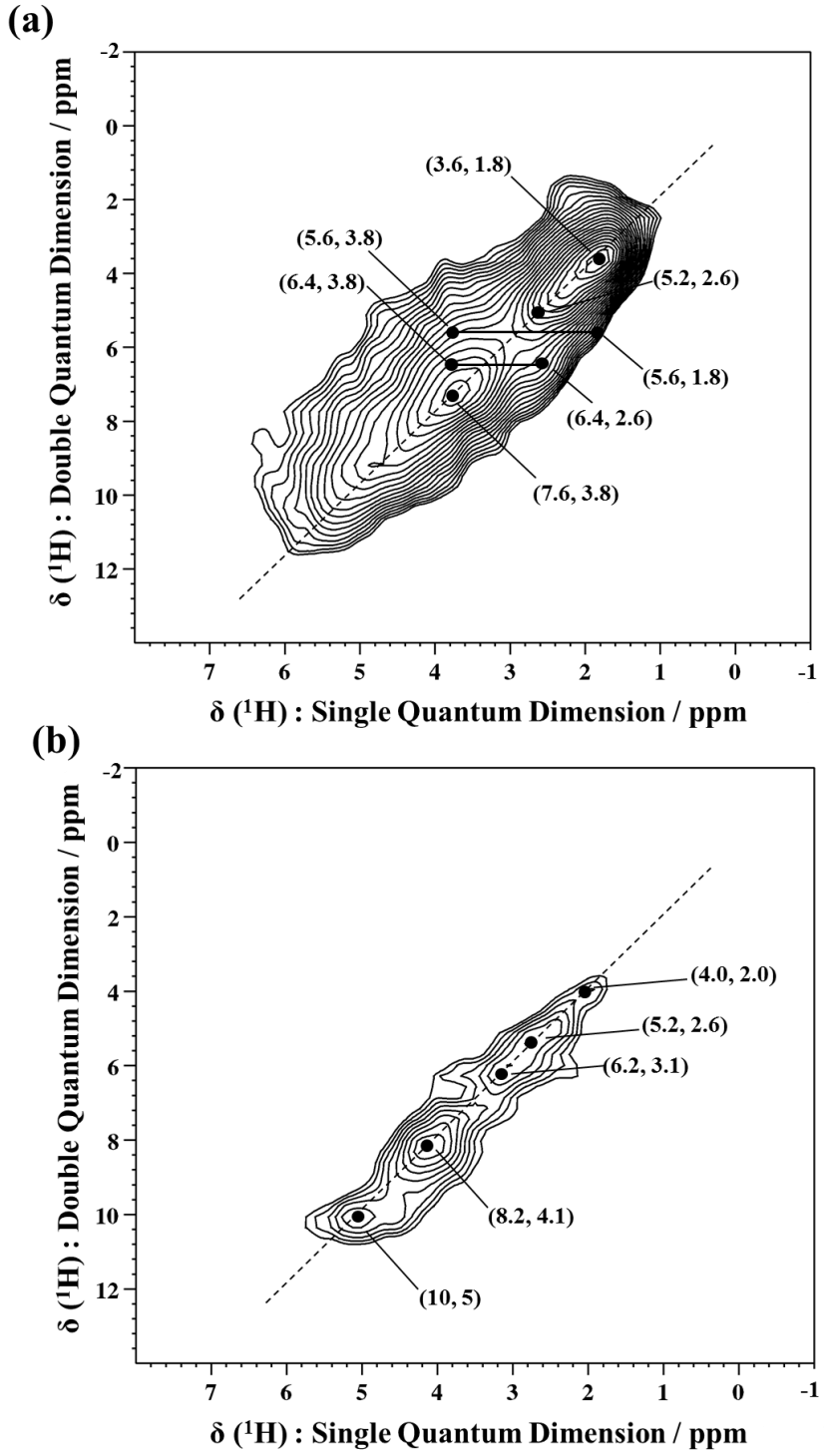

Figure 8. Two-dimensional ^{1}H DQ-SQ NMR spectra of (a) Z-25-Small and (b) Z-22-Big after activation at 300°C.

A third autocorrelation peak at (ω_1, ω_2) = (7.6 ppm, 3.8 ppm) is present. The 3.8 ppm chemical shift is somewhat lower than the 4.1 ppm peak observed in 1D ^{1}H NMR, assigned

from DFT calculations to bridging Si-(OH)-Al and isolated Al-(H_2O). In average (Table 3), isolated Al-(H_2O) species have been however predicted at lower chemical shift (at around 3.8 ppm) with respect to bridging OH groups (close or above 4 ppm). Thus, the autocorrelation peak can be confidently assigned to isolated Al-(H_2O) groups, in which the two very proximate (about 1.6 Å) protons correlate with the other (figure 9-c). It is interesting to see that if one-dimensional NMR spectroscopy merges the contributions from isolated Al-(H_2O) and bridging OH groups, ^{1}H DQ-SQ NMR is able to resolve the contribution of isolated Al-(H_2O) alone, as bridging OH groups are further from each other, and further from isolated Al-(H_2O) .

Two set of off-diagonal correlations are also visible at around (ω_1, ω_2) = (5.6 ppm, 3.8 ppm) and at (ω_1, ω_2) = (6.4 ppm, 2.6 ppm). The first one would correspond to proximities between protons at 3.8 and 1.8 ppm. As already discussed, 3.8 ppm corresponds to isolated Al-(H_2O) species. The signal around 1.8 ppm is due to isolated silanols and isolated Silanol-Al. This means that isolated Al-(H_2O) are close to isolated silanols (of all kinds) (Figure 9-a-b). The second off-diagonal correlation set corresponds to contacts between protons at around 3.8 and 2.6 ppm. The latter chemical shift has been previously assigned to Al-(H_2O) with one H-donor, hydrogen-bond acceptor silanols and μ_2-Al-OH. A proximity between isolated Al-(H_2O) species having a chemical shift at 3.8 pm and μ_2-Al-OH groups could be expected (as observed in the EFAl models, e.g. in Figure 2-c, although in this case the Al-(H_2O) species are hydrogen-bond donors). A proximity between isolated Al-(H_2O) and hydrogen-bond acceptor silanols is also expected (as depicted in Figure 9-b-c), that would also be compatible with the observation of these off-diagonal correlations.

For Z-22-Big (Figure 8-b), no off-diagonal correlations are observed. This could be explained by the very low amount of Al-(H_2O) species on that sample, due to its low external surface area. An autocorrelation peak at 4.1 ppm is observed, versus 3.8 ppm for Z-25-Small:

this suggests first that Al-(H_2O) are in strong minority with respect to bridging OH groups, in agreement with the 1D ^{1}H MAS NMR spectra. Second, this indicates that some of the bridging OH groups are close to each other and/or close to Al-(H_2O) species.

Notably, in many cases proximities between hydrogen-bond donor hydroxyls and other groups shall be seen, but their observation is not straightforward due to the width of the high chemical shift signals of the former. Also, 2MR sites (expected at 4.55 ppm) do not show any proximity with other protons, or are too diluted to make this observation feasible.

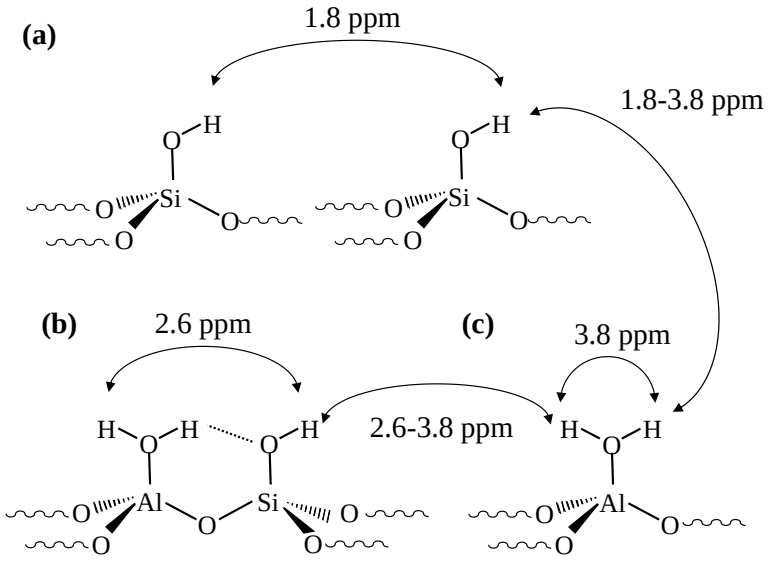

Figure 9. Simplified representation of the proximities observed by ^{1}H SQ-DQ NMR, for the sites that are specific to the external surface, as assigned by DFT. The value of ω_2 for the observed correlation is reported. (a) autocorrelation peak at (ω_1, ω_2) = (3.6 ppm, 1.8 ppm) due to the silanol network, (b) correlation peak at (ω_1, ω_2) = (5.2 ppm, 2.6 ppm), explained (inter alia) by the proximity between Al-(H_2O) and Silanol-Al, (c) autocorrelation peak at (ω_1, ω_2) = (7.6 ppm, 3.8 ppm), assigned to isolated Al-(H_2O). The contribution of extra-framework species are omitted for the sake of clarity.

In summary, the interpretation of the 2D ^{1}H-^{1}H through-space correlation spectra in the light of the assignment obtained from the DFT calculations brings new structural information summarized in Figure 9. More specifically, new details on the spectroscopic expression of the external surface sites are revealed thanks to this analysis, with particle size-dependent insights.

3.5. Towards the nature of the Al attached to OH bridging sites

To go further, from the absorbance of the contributions observed at 3745 and 3610 cm^{-1} for Z-22-Big and Z-25-Small (Figure 5a), it is possible to determine the molar concentrations of silanols and bridging sites, respectively (Table 4). Direct confrontation to ^{1}H MAS NMR results is not straightforward, since it would require a calibration in order to convert ^{1}H NMR signal into molar concentration. However, since quantification of NMR signal is not sensitive to the nature of the hydroxyl groups, IR and NMR results could be compared in terms of concentration ratio of the SiOHAl/SiOH species. The calculated ratios are highly consistent between both techniques : about 7 times more bridging sites than silanols are present for Z-22-Big.

Table 4. OH sites and Al^{IV} molar concentrations determined from ^{27}Al, ^{1}H NMR and IR spectroscopies on Z-22-Big and Z-25-Small after thermal activation at 573 K under vacuum (except for ^{27}Al NMR spectroscopy performed on hydrated samples).

	SiOH [a] (µmol/g)	SiOHAl [a] (µmol/g)	IR ratio [a] SiOHAl/SiOH	^{1}H NMR ratio [b] SiOHAl/SiOH	Al^{IV+VI} [c] µmol/g	Al^{IV} [d] µmol/g	Al^{IV}_{1} [d] µmol/g
Z-22-Big	81 +/-20	603	7.4	7.2	724	681	536
Z-25-Small	190 +/-20	235	1.2	0.8	641	641	276

[a] from IR analysis, using extinction coefficients from Gallas et al.[123] and Emeis[124]; [b] from ^{1}H NMR analysis; [c] determined from elemental composition from XRF analysis; [d] from ^{27}Al MQ-MAS NMR analysis.

Additionally, based on ^{27}Al MQ-MAS results, an attempt was made in order to indirectly obtain information on the nature of Al sites attached to the bridging OH sites (considering that hydrated state, favorable for ^{27}Al NMR analysis, does not affect the coordination of Al^{IV} species). In the present case of study, both samples report similar proportions and molar concentrations of tetra-coordinated Al^{IV} atoms (> 94% of total Al atoms as indicated in Table 1; ca. 650 µmol/g as shown in Table 4). If each Al^{IV} atom detected was connected to one OH bridging sites, one would expect very similar intensities of the signals at 3610 cm^{-1} (IR; Figure 5-a) and 4 ppm (^{1}H NMR; Figure 7-a) for both samples. But the situation is

significantly different, since Z-25-Small sample exhibits 60% less OH bridging sites compared to Z-22-Big zeolite. Thus, for Z-25-Small, only part of tetracoordinated Al^{IV} atoms (37%) are connected to bridging OH sites (88% for Z-22-Big).

Spectral resolution of ^{27}Al MQ-MAS measurements allowed one to distinguish three different framework Al^{IV} sites (Figures S4 an S5). The main population denoted as Al^{IV}_1 is centered at δ_{iso} = 54.0 ppm and 53.6 ppm for, respectively, Z-22-Big and Z-25-Small.For both zeolites, the two other signals (Al^{IV}_2 and Al^{IV}_3) are found at higher chemical shifts δ_{iso} = 55.4 and 57.0 ppm, respectively. According to ^{27}Al MQ-MAS, Al^{IV}_1 population represents about 74% and 43% of total Al atoms, which corresponds to concentrations of 536 and 276 µmol/g as indicated in Table 4 for Z-22-Big and Z-25-Small, respectively. The Al^{IV}_1 concentrations calculated from ^{27}Al MQMAS NMR for both zeolites are very close to those determined from IR spectroscopy (603 and 235 µmol/g) and suggest (from a quantitative point of view) that Al^{IV}_1 atoms are probably the ones that are connected to the OH bridging sites. On the other hand, the other tetra-coordinated Al^{IV} atoms are maybe linked to external surface and/or extra-framework Al species not prompt to create bridging sites as displayed in Figure 1.

3.6. Relation between infra-red and ^{1}H NMR features

Finally, we note that infrared and ^{1}H NMR spectroscopies provide consistent but complementary insights. Figure 103 reports the parity plot between the computed ^{1}H NMR chemical shift with the calculated O-H vibration frequency, for all the hydroxyl groups that have been investigated by both techniques in this study (notably, many more species have been the object of chemical shifts calculations). An expected trend appears, linking high frequencies with low chemical shifts. This trend is, however, rather approximate, showing that subtle structural effects play a different role from one technique to another. Combining

the two techniques is thus a way to detect differences between samples that cannot be seen with one technique only.

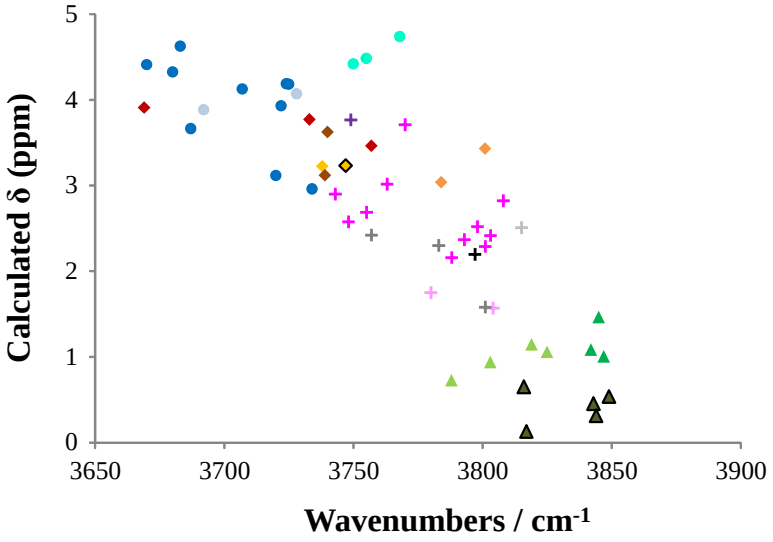

Figure 10. Correlation between computed proton chemical shifts and O-H vibration frequency for the same OH groups. The colour code is the same as in Figures 5 and 7.

4. CONCLUSION

The nature and spectroscopic expression of external surface sites of zeolites are a long-debated question, in particular for ZSM-5, one of the most popular zeolites, both from a fundamental and industrial point of view. In the present work, we have combined FTIR spectroscopy with Fourier self-deconvolution, high magnetic field ^{1}H solid-state NMR and periodic boundary DFT calculations on up-to-date external surface models to analyze the effect of crystallite size, so as to provide an exhaustive description of the various kinds of surface hydroxyl groups and of their proximities, with an unequaled level of detail. Notably, DFT calculations allowed the assignment of the experimentally-observed resonances to various types of OHs, whether isolated, donor or acceptor, while considering their location, i.e., in the bulk, at the external surface or as extra-framework species.

This analysis revealed that different types of OH groups usually contribute to a single NMR or IR resonance frequency. However, we have shown that when signals overlap with one spectroscopy, in most cases, they can be separated by the other technique, which further highlights the complementarity of the two experimental approaches used here. Thus, bridging Si-(OH)-Al and Al-(H_2O) groups lead to overlapping signals in 1D ^{1}H NMR spectra, whereas their resonances are strongly different in IR spectra. Similarly, bridging OH groups belonging to 2MR sites have the same NMR resonance as other bridging OH groups, whereas they exhibit a higher frequency in IR spectra. Hence, in these cases, identifying the nature of hydroxyl groups is somewhat easier by IR spectroscopy while their quantification and proximity assessment can better be obtained by ^{1}H NMR.

On the basis of our DFT calculations, conventional IR and NMR assignments have been revisited. While we confirmed previous proposals with regard to silanols and Si-(OH)-Al bridging OH groups, we observed that other signals (between 3750 and 3600 cm^{-1}, and between 1 and 4 ppm) cannot be assigned only to extra-framework species (which we confirm with dedicated models), but also enclose the signature of several types of sites exposed at the external surface of ZSM-5. In particular, Al-(H_2O) species (~3665 cm^{-1}, 3.8, 2.6 ppm) and Silanol-Al (~3740, 3720, 3665 cm^{-1}, 2.6, 2.2 ppm) contribute to several signals depending on their environment. μ_1-Al-OH are also present at the external surface in low amount, with a 3780 cm^{-1} signal in IR, and weak signals in the 0-2 ppm interval in ^{1}H NMR.

In summary, this work provides a refined analysis of the OH groups located at the external surface of ZSM-5, revealing the spectroscopic signature of groups such as Al-(H_2O), Silanol-A, and 2MR bridging OH, which are likely to play an important in role in catalysis. Applying this detailed analysis to other zeolites and aluminosilicates, is expected to help to better apprehend the active catalytic sites in these materials, and thereby to open new doors for structure-activity-reactivity relationships.

Supporting Information.

The following file is available free of charge: Supporting Informations.pdf (Additional structural DFT data, Main characteristics of the two zeolite samples, Additional Infrared data, Additional ^{1}H NMR data).

AUTHOR INFORMATION

Corresponding Author

* celine.chizallet@ifpen.fr

Present Addresses

† D. Wisser's present address: Erlangen Center for Interface Research and Catalysis, Friedrich-Alexander Universität Erlangen-Nürnberg, Egerlandstrasse 3, 91058 Erlangen, Germany

Author Contributions

‡These authors contributed equally.

ACKNOWLEDGMENT

This work was performed using HPC resources from GENCI (Grant A0020806134) and the ENER440 cluster at IFP Energies nouvelles. This work has been supported by the Common Research laboratory CARMEN (ENS de Lyon, CNRS, IFPEN, Claude Bernard Lyon 1 University, Sorbonne University and University of Strasbourg). Financial support from the TGIR-RMN-THC Fr3050 CNRS for conducting the research is also gratefully acknowledged.

REFERENCES

(1) Vermeiren, W.; Gilson, J. P., Impact of Zeolites on the Petroleum and Petrochemical Industry, *Topics Catal.* **2009**, *52*, 1131-1161.

(2) Marcilly, C. *Acido-Basic Catalysis*; Technip: Paris, 2005.

(3) Bertoncini, F.; Bonduelle-Skrzypcak, A.; Francis, J.; Guillon, E.,Hydrocracking, In *Catalysis by transition metal sulphides: from molecular theory to industrial applications*; Toulhoat, H., Raybaud, P., Eds.; Editions Technip: 2013, p 609-677.

(4) Ennaert, T.; Van Aelst, J.; Dijkmans, J.; De Clercq, R.; Schutyser, W.; Dusselier, M.; Verboekend, D.; Sels, B. F., Potential and Challenges of Zeolite Chemistry in the Catalytic Conversion of Biomass, *Chem. Soc. Rev.* **2016**, *45*, 584-611.

(5) Deka, U.; Lezcano-Gonzalez, I.; Weckhuysen, B. M.; Beale, A. M., Local Environment and Nature of Cu Active Sites in Zeolite-Based Catalysts for the Selective Catalytic Reduction of NOx, *ACS Catal.* **2013**, *3*, 413-427.

(6) Borfecchia, E.; Beato, P.; Svelle, S.; Olsbye, U.; Lamberti, C.; Bordiga, S., Cu-CHA – A Model System for Applied Selective Redox Catalysis, *Chem. Soc. Rev.* **2018**, *47*, 8097-8133.

(7) Argauer, R. J.; Landolt, G. R.; Mobil Oil Corporation: US 3702886, 1972.

(8) Roeffaers, M. B. J.; Ameloot, R.; Bons, A.-J.; Mortier, W.; De Cremer, G.; de Kloe, R.; Hofkens, J.; De Vos, D. E.; Sels, B. F., Relating Pore Structure to Activity at the Subcrystal Level for ZSM-5: An Electron Backscattering Diffraction and Fluorescence Microscopy Study, *J. Am. Chem. Soc.* **2008**, *130*, 13516-13517.

(9) Roeffaers, M. B. J.; Ameloot, R.; Baruah, M.; Uji-i, H.; Bulut, M.; De Cremer, G.; Müller, U.; Jacobs, P. A.; Hofkens, J.; Sels, B. F.; De Vos, D. E., Morphology of Large ZSM-5 Crystals Unraveled by Fluorescence Microscopy, *J. Am. Chem. Soc.* **2008**, *130*, 5763–5772.

(10) Roeffaers, M. B. J.; Sels, B. F.; Uji-i, H.; Blanpain, B.; L'Hoëst, P.; Jacobs, P. A.; De Schryver, F. C.; Hofkens, J.; De Vos, D. E., Space- and Time-Resolved Visualization of Acid Catalysis in ZSM-5 Crystals by Fluorescence Microscopy, *Angew. Chem. Int. Ed.* **2007**, *46*, 1706-1709.

(11) Karwacki, L.; de Winter, D. A. M.; Aramburo, L. R.; Lebbink, M. N.; Post, J. A.; Drury, M. R.; Weckhuysen, B. M., Architecture-Dependent Distribution of Mesopores in Steamed Zeolite Crystals as Visualized by FIB-SEM Tomography, *Angew. Chem. Int. Ed.* **2011**, *50*, 1294-1298.

(12) Karwacki, L.; Kox, M. H. F.; Matthijs de Winter, D. A.; Drury, M. R.; Meeldijk, J. D.; Stavitski, E.; Schmidt, W.; Mertens, M.; Cubillas, P.; John, N.; et al., Morphology-Dependent Zeolite Intergrowth Structures Leading to Distinct Internal and Outer-Surface Molecular Diffusion Barriers, *Nat. Mater.* **2009**, *8*, 959.

(13) Choi, M.; Na, K.; Kim, J.; Sakamoto, Y.; Terasaki, O.; Ryoo, R., Stable Single-Unit-Cell Nanosheets of Zeolite MFI as Active and Long-Lived Catalysts, *Nature* **2009**, *461*, 246-249.

(14) Varoon, K.; Zhang, X.; Elyassi, B.; Brewer, D. D.; Gettel, M.; Kumar, S.; Lee, J. A.; Maheshwari, S.; Mittal, A.; Sung, C.-Y.; et al., Dispersible Exfoliated Zeolite Nanosheets and Their Application as a Selective Membrane, *Science* **2011**, *334*, 72.

(15) Roth, W. J.; Nachtigall, P.; Morris, R. E.; Čejka, J., Two-Dimensional Zeolites: Current Status and Perspectives, *Chem. Rev.* **2014**, *114*, 4807-4837.

(16) Grand, J.; Talapaneni, S. N.; Vicente, A.; Fernandez, C.; Dib, E.; Aleksandrov, H. A.; Vayssilov, G. N.; Retoux, R.; Boullay, P.; Gilson, J.-P.; et al., One-Pot Synthesis of Silanol-Free Nanosized MFI Zeolite, *Nat. Mater.* **2017**, *16*, 1010-1015.

(17) Mintova, S.; Jaber, M.; Valtchev, V., Nanosized Microporous Crystals: Emerging Applications, *Chem. Soc. Rev.* **2015**, *44*, 7207-7233.
(18) Haw, K.-G.; Gilson, J.-P.; Nesterenko, N.; Akouche, M.; El Siblani, H.; Goupil, J.-M.; Rigaud, B.; Minoux, D.; Dath, J.-P.; Valtchev, V., Supported Embryonic Zeolites and their Use to Process Bulky Molecules, *ACS Catal.* **2018**, *8*, 8199-8212.
(19) Haw, K.-G.; Goupil, J.-M.; Gilson, J.-P.; Nesterenko, N.; Minoux, D.; Dath, J.-P.; Valtchev, V., Embryonic ZSM-5 Zeolites: Zeolitic Materials with Superior Catalytic Activity in 1,3,5-Triisopropylbenzene Dealkylation, *New J. Chem.* **2016**, *40*, 4307-4313.
(20) Martens, J. A.; Vanbutsele, G.; Jacobs, P. A.; Denayer, J.; Ocakoglu, R.; Baron, G.; Muñoz Arroyo, J. A.; Thybaut, J.; Marin, G. B., Evidences for Pore Mouth and Key–Lock Catalysis in Hydroisomerization of Long n-Alkanes over 10-Ring Tubular Pore Bifunctional Zeolites, *Catal. Today* **2001**, *65*, 111-116.
(21) Martens, J. A.; Souverijns, W.; Verrelst, W.; Parton, R.; Froment, G. F.; Jacobs, P. A., Selective Isomerization of Hydrocarbon Chains on External Surfaces of Zeolite Crystals, *Angew. Chem. Int. Ed.* **1995**, *34*, 2528-2530.
(22) Radhakrishnan, S.; Goossens, P. J.; Magusin, P. C.; Sree, S. P.; Detavernier, C.; Breynaert, E.; Martineau, C.; Taulelle, F.; Martens, J. A., In Situ Solid-State ^{13}C NMR Observation of Pore Mouth Catalysis in Etherification of beta-Citronellene with Ethanol on Zeolite Beta, *J. Am. Chem. Soc.* **2016**, *138*, 2802-2808.
(23) Moreau, F.; Moreau, P.; Gnep, N. S.; Magnoux, P.; Lacombe, S.; Guisnet, M., Ethylbenzene Isomerization over Bifunctional Platinum Alumina–EUO Catalysts: Location of the Active Sites, *Microporous Mesoporous Mater.* **2006**, *90*, 327-338.
(24) Zecevic, J.; Vanbutsele, G.; de Jong, K. P.; Martens, J. A., Nanoscale Intimacy in Bifunctional Catalysts for Selective Conversion of Hydrocarbons, *Nature* **2015**, *528*, 245-248.
(25) Chizallet, C., Towards the Atomic Scale Simulation of Intricate Zeolitic Acidic Catalysts, *ACS Catal.* **2020**.
(26) Rey, J.; Raybaud, P.; Chizallet, C., Ab Initio Simulation of the Acid Sites at the External Surface of Zeolite Beta, *ChemCatChem* **2017**, *9*, 2176-2185.
(27) Treps, L.; Gomez, A.; De Bruin, T.; Chizallet, C., Environment, Stability and Acidity of External Surface Sites of Silicalite-1 and ZSM-5 Micro- and Nano-Slabs, -Sheets and -Crystals, *ACS Catal.* **2020**, *10*, 3297−3312.
(28) Chizallet, C.; Raybaud, P., Acidity of Amorphous Silica–Alumina: From Coordination Promotion of Lewis Sites to Proton Transfer, *ChemPhysChem* **2010**, *11*, 105-108.
(29) Leydier, F.; Chizallet, C.; Chaumonnot, A.; Digne, M.; Soyer, E.; Quoineaud, A. A.; Costa, D.; Raybaud, P., Brønsted Acidity of Amorphous Silica–Alumina: The Molecular Rules of Proton Transfer, *J. Catal.* **2011**, *284*, 215-229.
(30) Hadjiivanov, K.,Chapter Two - Identification and Characterization of Surface Hydroxyl Groups by Infrared Spectroscopy, In *Adv. Catal.*; Jentoft, F. C., Ed.; Academic Press: 2014; Vol. 57, p 99-318.
(31) Bordiga, S.; Lamberti, C.; Bonino, F.; Travert, A.; Thibault-Starzyk, F., Probing Zeolites by Vibrational Spectroscopies, *Chem. Soc. Rev.* **2015**, *44*, 7262-7341.
(32) Védrine, J. C.; Auroux, A.; Bolis, V.; Dejaifve, P.; Naccache, C.; Wierzchowski, P.; Derouane, E. G.; Nagy, J. B.; Gilson, J.-P.; van Hooff, J. H. C.; et al., Infrared, Microcalorimetric, and Electron Spin Resonance Investigations of the Acidic Properties of the H-ZSM-5 Zeolite, *J. Catal.* **1979**, *59*, 248-262.
(33) Topsøe, N.-Y.; Pedersen, K.; Derouane, E. G., Infrared and Temperature-Programmed Desorption Study of the Acidic Properties of ZSM-5-Type Zeolites, *J. Catal.* **1981**, *70*, 41-52.

(34) Jacobs, P. A.; Von Ballmoos, R., Framework Hydroxyl Groups of H-ZSM-5 Zeolites, *J. Phys. Chem.* **1982**, *86*, 3050-3052.
(35) Datka, J.; Gil, B.; Baran, P., Heterogeneity of OH Groups in HZSM-5 Zeolites: Splitting of OH and OD Bands in Low-Temperature IR Spectra, *Microporous Mesoporous Mater.* **2003**, *58*, 291-294.
(36) Armaroli, T.; Simon, L. J.; Digne, M.; Montanari, T.; Bevilacqua, M.; Valtchev, V.; Patarin, J.; Busca, G., Effects of Crystal Size and Si/Al Ratio on the Surface Properties of H-ZSM-5 Zeolites, *Appl. Catal. A* **2006**, *306*, 78-84.
(37) Zecchina, A.; Bordiga, S.; Spoto, G.; Marchese, L.; Petrini, G.; Leofanti, G.; Padovan, M., Silicalite Characterization. 2. IR Spectroscopy of the Interaction of Carbon Monoxide with Internal and External Hydroxyl Groups, *J. Phys. Chem.* **1992**, *96*, 4991-4997.
(38) Lonstad Bleken, B.-T.; Mino, L.; Giordanino, F.; Beato, P.; Svelle, S.; Lillerud, K. P.; Bordiga, S., Probing the Surface of Nanosheet H-ZSM-5 with FTIR Spectroscopy, *Phys. Chem. Chem. Phys.* **2013**, *15*, 13363-13370.
(39) Holm, M. S.; Svelle, S. J. F.; Beato, P.; Christensen, C. H.; Bordiga, S.; Bjørgen, M., Assessing the Acid Properties of Desilicated ZSM-5 by FTIR using CO and 2,4,6-Trimethylpyridine (Collidine) as Molecular Probes, *Appl. Catal. A* **2009**, *356*, 23-30.
(40) Brus, J.; Kobera, L.; Schoefberger, W.; Urbanova, M.; Klein, P.; Sazama, P.; Tabor, E.; Sklenak, S.; Fishchuk, A. V.; Dedecek, J., Structure of Framework Aluminum Lewis sites and Perturbed Aluminum atoms in Zeolites as Determined by $^{27}Al\{^{1}H\}$ REDOR (3Q) MAS NMR Spectroscopy and DFT/Molecular Mechanics, *Angew. Chem. Int. Ed.* **2015**, *54*, 541-545.
(41) Osuga, R.; Yokoi, T.; Doitomi, K.; Hirao, H.; Kondo, J. N., Infrared Investigation of Dynamic Behavior of Brønsted Acid Sites on Zeolites at High Temperatures, *J. Phys. Chem. C* **2017**, *121*, 25411-25420.
(42) Losch, P.; Joshi, H. R.; Vozniuk, O.; Grunert, A.; Ochoa-Hernandez, C.; Jabraoui, H.; Badawi, M.; Schmidt, W., Proton Mobility, Intrinsic Acid Strength and Acid Site Location in Zeolites Revealed by VTIR and DFT Studies, *J. Am. Chem. Soc.* **2018**.
(43) Hoffmann, P.; Lobo, J. A., Identification of Diverse Silanols on Protonated ZSM-5 Zeolites by Means of FTIR Spectroscopy, *Microporous Mesoporous Mater.* **2007**, *106*, 122-128.
(44) Dessau, R. M.; Schmitt, K. D.; Kerr, G. T.; Woolery, G. L.; Alemany, L. B., On the Presence of Internal Silanol Groups in ZSM-5 and the Annealing of these Sites by Steaming, *J. Catal.* **1987**, *104*, 484-489.
(45) Crépeau, G.; Montouillout, V.; Vimont, A.; Mariey, L.; Cseri, T.; Maugé, F., Nature, Structure and Strength of the Acidic Sites of Amorphous Silica Alumina: an IR and NMR Study, *J. Phys. Chem. B* **2006**, *110*, 15172-15185.
(46) Zholobenko, V.; Freitas, C.; Jendrlin, M.; Bazin, P.; Travert, A.; Thibault-Starzyk, F., Probing the Acid Sites of Zeolites with Pyridine: Quantitative AGIR Measurements of the Molar Absorption Coefficients, *J. Catal.* **2020**, *385*, 52-60.
(47) Lippmaa, E.; Samoson, A.; Mägi, M., High-Resolution 27Al NMR of Aluminosilicates, *J. Am. Chem. Soc.* **1986**, *108*, 1730-1735.
(48) Frydman, L.; Harwood, J. S., Isotropic Spectra of Half-Integer Quadrupolar Spins from Bidimensional Magic-Angle Spinning NMR, *J. Am. Chem. Soc.* **1995**, *117*, 5367-5368.
(49) Fernandez, C.; Amoureux, J. P., Triple-Quantum MAS-NMR of Quadrupolar Nuclei, *Solid State Nucl. Magn. Reson.* **1996**, *5*, 315-321.
(50) Sarv, P.; Fernandez, C.; Amoureux, J.-P.; Keskinen, K., Distribution of Tetrahedral Aluminium Sites in ZSM-5 Type Zeolites: An ^{27}Al (Multiquantum) Magic Angle Spinning NMR Study, *J. Phys. Chem.* **1996**, *100*, 19223-19226.

(51) Han, O. H.; Kim, C. S.; Hong, S. B., Direct Evidence for the Nonrandom Nature of Al Substitution in Zeolite ZSM-5: An Investigation by ^{27}Al MAS and MQ MAS NMR, *Angew. Chem. Int. Ed.* **2002**, *41*, 469-472.
(52) Holzinger, J.; Beato, P.; Lundegaard, L. F.; Skibsted, J., Distribution of Aluminum over the Tetrahedral Sites in ZSM-5 Zeolites and Their Evolution after Steam Treatment, *J. Phys. Chem. C* **2018**, *122*, 15595-15613.
(53) Freude, D.; Hunger, M.; Pfeifer, H.; Schwieger, W., ^{1}H MAS NMR Studies on the Acidity of Zeolites, *Chem. Phys. Lett.* **1986**, *128*, 62-66.
(54) Engelhardt, G.; Jerschkewitz, H. G.; Lohse, U.; Sarv, P.; Samoson, A.; Lippmaa, E., 500 MHz ^{1}H-MAS N.M.R. Studies of Dealuminated HZSM-5 Zeolites, *Zeolites* **1987**, *7*, 289-292.
(55) Beck, L. W.; White, J. L.; Haw, J. F., ^{1}H{^{27}Al} Double-Resonance Experiments in Solids: An Unexpected Observation in the ^{1}H MAS Spectrum of Zeolite HZSM-5, *J. Am. Chem. Soc.* **1994**, *116*, 9657-9661.
(56) Freude, D., Enhanced Resolution in the ^{1}H NMR Spectra of Zeolite H-ZSM-5 by Heteronuclear Dipolar-Dephasing Spin-Echo MAS, *Chem. Phys. Lett.* **1995**, *235*, 69-75.
(57) Hunger, M., Multinuclear Solid-State NMR Studies of Acidic and Non-Acidic Hydroxyl Protons in Zeolites, *Solid State Nucl. Magn. Reson.* **1996**, *6*, 1-29.
(58) Brunner, E.; Beck, K.; Koch, M.; Heeribout, L.; Karge, H. G., Verification and Quantitative Determination of a New Type of Brønsted Acid Sites in H-ZSM-5 by ^{1}H Magic-Angle Spinning Nuclear Magnetic Resonance Spectroscopy, *Micropor. Mater.* **1995**, *3*, 395-399.
(59) Baba, T.; Ono, Y., Dynamic Properties of Protons in Solid Acids as Studied by Variable Temperature ^{1}H MAS NMR, *Appl. Catal. A* **1999**, *181*, 227-238.
(60) Huo, H.; Peng, L.; Grey, C. P., Low Temperature ^{1}H MAS NMR Spectroscopy Studies of Proton Motion in Zeolite HZSM-5, *J. Phys. Chem. C* **2009**, *113*, 8211-8219.
(61) Louis, B.; Vicente, A. l.; Fernandez, C.; Valtchev, V., Crystal Size–Acid Sites Relationship Study of Nano- and Micrometer-Sized Zeolite Crystals, *J. Phys. Chem. C* **2011**, *115*, 18603-18610.
(62) Wang, M.; Jaegers, N. R.; Lee, M. S.; Wan, C.; Hu, J. Z.; Shi, H.; Mei, D.; Burton, S. D.; Camaioni, D. M.; Gutierrez, O. Y.; et al., Genesis and Stability of Hydronium Ions in Zeolite Channels, *J. Am. Chem. Soc.* **2019**, *141*, 3444-3455.
(63) Poirier, M.; Millot, Y.; Silva Gomes, E.; Jaber, M.; Herledan, V.; Laugel, G.; Micoud, P.; Martin, F.; Lauron-Pernot, H.; Toulhoat, H., Complementarity of Density Functional Theory and Nuclear Magnetic Resonance Tools To Probe the Nano-Layered Silicates Surface Chemistry and Morphology, *J. Phys. Chem. C* **2019**, *124*, 267-286.
(64) Hunger, M., Brønsted Acid Sites in Zeolites Characterized by Multinuclear Solid-State NMR Spectroscopy, *Catal. Rev.* **1997**, *39*, 345-393.
(65) Deng, F.; Yue, Y.; Ye, C., ^{1}H/^{27}Al TRAPDOR NMR Studies on Aluminum Species in Dealuminated Zeolites, *Solid State Nucl. Magn. Reson.* **1998**, *10*, 151-160.
(66) Seiler, M.; Wang, W.; Hunger, M., Local Structure of Framework Aluminum in Zeolite H−ZSM-5 during Conversion of Methanol Investigated by In Situ NMR Spectroscopy, *J. Phys. Chem. B* **2001**, *105*, 8143-8148.
(67) Chen, K.; Abdolrhamani, M.; Sheets, E.; Freeman, J.; Ward, G.; White, J. L., Direct Detection of Multiple Acidic Proton Sites in Zeolite HZSM-5, *J. Am. Chem. Soc.* **2017**, *139*, 18698-18704.
(68) Chen, K.; Horstmeier, S.; Nguyen, V. T.; Wang, B.; Crossley, S. P.; Pham, T.; Gan, Z.; Hung, I.; White, J. L., Structure and Catalytic Characterization of a Second Framework Al(IV) Site in Zeolite Catalysts Revealed by NMR at 35.2 T, *J. Am. Chem. Soc.* **2020**.

(69) Paul, G.; Bisio, C.; Braschi, I.; Cossi, M.; Gatti, G.; Gianotti, E.; Marchese, L., Combined Solid-State NMR, FT-IR and Computational Studies on Layered and Porous Materials, *Chem. Soc. Rev.* **2018**, *47*, 5684-5739.
(70) Brown, S. P.; Spiess, H. W., Advanced Solid-State NMR Methods for the Elucidation of Structure and Dynamics of Molecular, Macromolecular, and Supramolecular Systems, *Chem. Rev.* **2001**, *101*, 4125-4156.
(71) Yu, Z.; Li, S.; Wang, Q.; Zheng, A.; Jun, X.; Chen, L.; Deng, F., Brønsted/Lewis Acid Synergy in H–ZSM-5 and H–MOR Zeolites Studied by ^{1}H and ^{27}Al DQ-MAS Solid-State NMR Spectroscopy, *J. Phys. Chem. C* **2011**, *115*, 22320-22327.
(72) Xue, N.; Vjunov, A.; Schallmoser, S.; Fulton, J. L.; Sanchez-Sanchez, M.; Hu, J. Z.; Mei, D.; Lercher, J. A., Hydrolysis of Zeolite Framework Aluminum and its Impact on Acid Catalyzed Alkane Reactions, *J. Catal.* **2018**, *365*, 359-366.
(73) Bonhomme, C.; Gervais, C.; Babonneau, F.; Coelho, C.; Pourpoint, F.; Azais, T.; Ashbrook, S. E.; Griffin, J. M.; Yates, J. R.; Mauri, F.; et al., First-Principles Calculation of NMR Parameters Using the Gauge Including Projector Augmented Wave Method: A Chemist's Point of View, *Chem Rev* **2012**, *112*, 5733-5779.
(74) Bucko, T.; Benco, L.; Hafner, J., Defect Sites at the (001) Surface of Mordenite: An Ab Initio Study, *J. Chem. Phys.* **2003**, *118*, 8437-8445.
(75) Bucko, T.; Benco, L.; Demuth, T.; Hafner, J., Ab Initio Density Functional Investigation of the (001) Surface of Mordenite, *J. Chem. Phys.* **2002**, *117*, 7295-7305.
(76) Batista, A. T. F.; Wisser, D.; Pigeon, T.; Gajan, D.; Diehl, F.; Rivallan, M.; Catita, L.; Gay, A.-S.; Lesage, A.; Chizallet, C.; et al., Beyond γ-Al_2O_3 Crystallite Surfaces: The Hidden Features of Edges Revealed by Solid-State ^{1}H NMR and DFT Calculations, *J. Catal.* **2019**, *378*, 140-143.
(77) Chizallet, C.; Costentin, G.; Lauron-Pernot, H.; Che, M.; Bonhomme, C.; Maquet, J.; Delbecq, F.; Sautet, P., 1D and 2D ^{1}H MAS NMR Structural Investigation of OH Groups on MgO by a Combination of Experiments and Theory, *J. Phys. Chem. C* **2007**, *111*, 18279-18287.
(78) Chizallet, C.; Costentin, G.; Che, M.; Delbecq, F.; Sautet, P., Infra-Red Characterization of Hydroxyl Groups on MgO: a Periodic and Cluster DFT Study, *J. Am. Chem. Soc.* **2007**, *129*, 6442-6452.
(79) Digne, M.; Sautet, P.; Raybaud, P.; Euzen, P.; Toulhoat, H., Use of DFT to Achieve a Rational Understanding of Acid–Basic Properties of Gamma-Alumina Surfaces, *J. Catal.* **2004**, *226*, 54-68.
(80) Arrouvel, C.; Digne, M.; Breysse, M.; Toulhoat, H.; Raybaud, P., Effects of Morphology on Surface Hydroxyl Concentration: a DFT Comparison of Anatase–TiO_2 and γ-Alumina Catalytic Supports, *J. Catal.* **2004**, *222*, 152-166.
(81) Tielens, F.; Gervais, C.; Lambert, J. F.; Mauri, F.; Costa, D., Ab Initio Study of the Hydroxylated Surface of Amorphous Silica: A Representative Model, *Chem. Mater.* **2008**, *20*, 3336-3344.
(82) Sastre, G.; Katada, N.; Niwa, M., Computational Study of Brønsted Acidity of Mordenite. Effect of the Electric Field on the Infrared OH Stretching Frequencies, *J. Phys. Chem. C* **2010**, *114*, 15424-15431.
(83) Islam, M. M.; Costa, D.; Calatayud, M.; Tielens, F., Characterization of Supported Vanadium Oxide Species on Silica: A Periodic DFT Investigation, *J. Phys. Chem. C* **2009**, *113*, 10740-10746.
(84) Tosoni, S.; Pascale, F.; Ugliengo, P.; Orlando, R.; Saunders, V. R.; Dovesi, R., Quantum Mechanical Calculation of the OH Vibrational Frequency in Crystalline Solids, *Mol. Phys.* **2005**, *103*, 2549-2558.

(85) Mortier, W. J.; Sauer, J.; Lercher, J. A.; Noller, H., Bridging and Terminal Hydroxyls. A Structural Chemical and Quantum Chemical Discussion, *J. Phys. Chem.* **1984**, *88*, 905-912.
(86) Fleischer, U.; Kutzelnigg, W.; Bleiber, A.; Sauer, J., ^{1}H NMR Chemical Shift and Intrinsic Acidity of Hydroxyl Groups. Ab Initio Calculations on Catalytically Active Sites and Gas-Phase Molecules, *J. Am. Chem. Soc.* **1993**, *115*, 7833-7838.
(87) Schroeder, C.; Siozios, V.; Mück-Lichtenfeld, C.; Hunger, M.; Hansen, M. R.; Koller, H., Hydrogen Bond Formation of Brønsted Acid Sites in Zeolites, *Chem. Mater.* **2020**, *32*, 1564-1574.
(88) Perdew, J.; Burke, K.; Ernzerhof, M., Generalized Gradient Approximation Made Simple, *Phys. Rev. Lett.* **1996**, *77*, 3865-3868.
(89) Kresse, G.; Hafner, J., Ab Initio Molecular-Dynamics Simulation of the Liquid-Metal-Amorphous-Semiconductor Transition in Germanium, *Phys. Rev. B* **1994**, *49*, 14251-14269.
(90) Kresse, G.; Furthmüller, J., Efficiency of Ab-Initio Total Energy Calculations for Metals and Semiconductors using a Plane-Wave Basis Set, *Comput. Mat. Sci.* **1996**, *6*, 15-50.
(91) Kresse, G.; Joubert, D., From Ultrasoft Pseudopotentials to the Projector Augmented-Wave Method, *Phys. Rev. B* **1999**, *59*, 1758-1775.
(92) Steinmann, S. N.; Corminboeuf, C., Comprehensive Benchmarking of a Density-Dependent Dispersion Correction, *J Chem Theory Comput* **2011**, *7*, 3567-3577.
(93) Baerlocher, C.; McCusker, J. K., *Database of Zeolite Structures:* http://www.iza-structure.org/databases/.
(94) Wu, E. L.; Lawton, S. L.; Olson, D. H.; Rohrman, A. C.; Kokotailo, G. T., ZSM-5-Type Materials. Factors Affecting Crystal Symmetry, *J. Phys. Chem.* **1979**, *83*, 2777-2781.
(95) Olson, D. H.; Kokotailo, G. T.; Lawton, S. L.; Meier, W. M., Crystal Structure and Structure-Related Properties of ZSM-5, *J. Phys. Chem.* **1981**, *85*, 2238-2243.
(96) Koegler, J. H.; van Bekkum, H.; Jansen, J. C., Growth Model of Oriented Crystals of Zeolite Si-ZSM-5, *Zeolites* **1997**, *19*, 262-269.
(97) Zeng, G.; Chen, C.; Li, D.; Hou, B.; Sun, Y., Exposure of (001) Planes and (011) Planes in MFI Zeolite, *CrystEngComm* **2013**, *15*, 3521-3524.
(98) Yates, J. R.; Pickard, C. J.; Mauri, F., Calculation of NMR Chemical Shifts for Extended Systems using Ultrasoft Pseudopotentials, *Phys. Rev. B* **2007**, *76*, 024401:024401-024411.
(99) Pickard, C. J.; Mauri, F., All-Electron Magnetic Response with Pseudopotentials: NMR Chemical Shifts, *Phys. Rev. B* **2001**, *63*, 245101.
(100) Amoureux, J.-P.; Fernandez, C.; Steuernagel, S., ZFiltering in MQMAS NMR, *J. Magn. Reson. A* **1996**, *123*, 116-118.
(101) Massiot, D., Sensitivity and Lineshape Improvements of MQ-MAS by Rotor-Synchronized Data Acquisition, *J. Magn. Reson. A* **1996**, *122*, 240-244.
(102) Massiot, D.; Fayon, F.; Capron, M.; King, I.; Le Calvé, S.; Alonso, B.; Durand, J. O.; Bujoli, B.; Gan, Z.; Hoatson, G., Modelling One- and Two-Dimensional Solid-State NMR Spectra, *Magn. Reson. Chem.* **2002**, *40*, 70-76.
(103) Robin Bendall, M.; Gordon, R. E., Depth and Refocusing Pulses Designed for Multipulse NMR with Surface Coils, *J. Magn. Reson.* **1983**, *53*, 365-385.
(104) Bendall, M. R.; Pegg, D. T., Theoretical Description of Depth Pulse Sequences, On and Off Resonance, Including Improvements and Extensions Thereof, *Magn. Reson. Med.* **1985**, *2*, 91-113.
(105) Cory, D. G.; Ritchey, W. M., Suppression of Signals from the Probe in Bloch Decay Spectra, *J. Magn. Reson.* **1988**, *80*, 128-132.

(106) Sommer, W.; Gottwald, J.; Demco, D. E.; Spiess, H. W., Dipolar Heteronuclear Multiple-Quantum NMR Spectroscopy in Rotating Solids, *J. Magn. Reson. A* **1995**, *113*, 131-134.
(107) Hernandez-Tamargo, C. E.; Roldan, A.; de Leeuw, N. H., A Density Functional Theory Study of the Structure of Pure-Silica and Aluminium-Substituted MFI Nanosheets, *J. Solid State Chem.* **2016**, *237*, 192-203.
(108) Song, W.; Justice, R. E.; Jones, C. A.; Grassian, V. H.; Larsen, S. C., Size-Dependent Properties of Nanocrystalline Silicalite Synthesized with Systematically Varied Crystal Sizes, *Langmuir* **2004**, *20*, 4696-4702.
(109) Pereira, M. M.; Gomes, E. S.; Silva, A. V.; Pinar, A. B.; Willinger, M.-G.; Shanmugam, S.; Chizallet, C.; Laugel, G.; Losch, P.; Louis, B., Biomass-Mediated ZSM-5 Zeolite Synthesis: When Self-Assembly Allows to Cross the Si/Al Lower Limit, *Chem. Sci.* **2018**, *9*, 6532-6539.
(110) Flanigen, E. M.; Bennett, J. M.; Grose, R. W.; Cohen, J. P.; Patton, R. L.; Kirchner, R. M.; Smith, J. V., Silicalite, a New Hydrophobic Crystalline Silica Molecular Sieve, *Nature* **1978**, *271*, 512-516.
(111) Vazhnova, T.; Lukyanov, D. B., Fourier Self-Deconvolution of the IR Spectra as a Tool for Investigation of Distinct Functional Groups in Porous Materials: Brønsted Acid Sites in Zeolites, *Anal. Chem.* **2013**, *85*, 11291-11296.
(112) Chizallet, C.; Digne, M.; Arrouvel, C.; Raybaud, P.; Delbecq, F.; Costentin, G.; Che, M.; Sautet, P.; Toulhoat, H., Insights into the Geometry, Stability and Vibrational Properties of OH Groups on γ-Al_2O_3, TiO_2-Anatase and MgO from DFT Calculations, *Topics Catal.* **2009**, *52*, 1005-1016.
(113) Jones, A. J.; Iglesia, E., The Strength of Brønsted Acid Sites in Microporous Aluminosilicates, *ACS Catal.* **2015**, *5*, 5741-5755.
(114) Loeffler, E.; Lohse, U.; Peuker, C.; Oehlmann, G.; Kustov, L. M.; Zholobenko, V. L.; Kazansky, V. B., Study of Different States of Nonframework Aluminum in Hydrothermally Dealuminated HZSM-5 Zeolites using Diffuse Reflectance i.r. Spectroscopy, *Zeolites* **1990**, *10*, 266-271.
(115) Jia, C.; Massiani, P.; Barthomeuf, D., Characterization by Infrared and Nuclear Magnetic Resonance Spectroscopies of Calcined Beta Zeolite, *J. Chem. Soc., Faraday Trans.* **1993**, *89*, 3659-3665.
(116) Zecchina, A.; Bordiga, S.; Spoto, G.; Scarano, D.; Petrini, G.; Leofanti, G.; Padovan, M.; Areàn, C. O., Low-Temperature Fourier-Transform Infrared Investigation of the Interaction of CO with Nanosized ZSM5 and Silicalite, *J. Chem. Soc., Faraday Trans.* **1992**, *88*, 2959-2969.
(117) Digne, M.; Sautet, P.; Raybaud, P.; Euzen, P.; Toulhoat, H., Hydroxyl Groups on Gamma-Alumina Surfaces: a DFT Study, *J. Catal.* **2002**, *211*, 1-5.
(118) Zholobenko, V. L.; Kustov, L. M.; Kazansky, V. B.; Loeffler, E.; Lohser, U.; Peuker, C.; Oehlmann, G., On the Possible Nature of Sites Responsible for the Enhancement of Cracking Activity of HZSM-5 Zeolites Dealuminated under Mild Steaming Conditions, *Zeolites* **1990**, *10*, 304-306.
(119) Szanyi, J.; Paffett, M. T., The Adsorption of Carbon Monoxide on H-ZSM-5 and Hydrothermally Treated H-ZSM-5, *Micropor. Mater.* **1996**, *7*, 201-218.
(120) Vimont, A.; Lavalley, J. C.; Thibault-Starzyk, F., Infrared Spectroscopic Study of the Acidobasic Properties of Beta Zeolite, *J. Phys. Chem. B* **2000**, *104*, 286-291.
(121) Zecchina, A.; Geobaldo, F.; Spoto, G.; Bordiga, S.; Ricchiardi, G.; Buzzoni, R.; Petrini, G., FTIR Investigation of the Formation of Neutral and Ionic Hydrogen-Bonded Complexes by Interaction of H-ZSM-5 and H-Mordenite with CH_3CN and H_2O:

Comparison with the H-NAFION Superacidic System, *J. Phys. Chem.* **1996**, *100*, 16584-16599.
(122) Jiao, J.; Altwasser, S.; Wang, W.; Weitkamp, J.; Hunger, M., State of Aluminum in Dealuminated, Nonhydrated Zeolites Y Investigated by Multinuclear Solid-State NMR Spectroscopy, *J. Phys. Chem. B* **2004**, *108*, 14305-14310.
(123) Gallas, J. P.; Lavalley, J. C.; Burneau, A.; Barres, O., Comparative Study of the Surface Hydroxyl Groups of Fumed and Precipitated Silicas. 4. Infrared Study of Dehydroxylation by Thermal Treatments, *Langmuir* **1991**, *7*, 1235-1240.
(124) Emeis, C. A., Determination of Integrated Molar Extinction Coefficients for Infrared Absorption Bands of Pyridine Adsorbed on Solid Acid Catalysts, *J. Catal.* **1993**, *141*, 347-354.

Graphical TOC: